



Synthesis and evaluation of the epithelial-to-mesenchymal inhibitory activity of indazole-derived imidazoles as dual ALK5/p38 α MAP inhibitors



Yue Ying Liu¹, Zhen Guo¹, Jing Ying Wang, Hui Min Wang, Jun Da Qi, Juan Ma, Hu-Ri Piao, Cheng Hua Jin^{*}, Xuejun Jin^{**}

Key Laboratory of Natural Resources of Changbai Mountain and Functional Molecules, Ministry of Education, Molecular Medicine Research Center, College of Pharmacy, Yanbian University, Yanji, 133002, PR China

ARTICLE INFO

Article history:

Received 29 November 2020

Received in revised form

15 February 2021

Accepted 15 February 2021

Available online 23 February 2021

Keywords:

ALK5

TGF- β

Imidazole

Inhibitors

EMT

Glioma

ABSTRACT

Drugs of targeting both activin receptor-like kinase 5 (ALK5) and p38 α have therapeutic advantages, making them attractive treatment options for tumors. Two series of 4-(1H-indazol-5-yl)-5-(6-methylpyridin-2-yl)-1H-imidazoles 13a–g and 4-(1-methyl-1H-indazol-5-yl)-5-(6-methylpyridin-2-yl)-1H-imidazoles 20a–g were synthesized and evaluated for ALK5 and p38 α mitogen-activated protein kinase inhibitory activity. The most potent compound, 13c (J-1090), inhibited ALK5- and p38 α -mediated phosphorylation with half-maximal inhibitor concentrations of 0.004 μ M and 0.004 μ M, respectively, in the enzymatic assay. In this study, the effectiveness of 13c in transforming growth factor (TGF- β)-exposed U87MG cells was investigated using western blotting, immunofluorescence assays, cell migration assay, invasion assay, and RT-PCR analysis. 13c inhibited the protein expression of Slug and the protein and RNA expression of the mesenchymal-related proteins N-cadherin and vimentin. Furthermore, 13c markedly suppressed TGF- β -induced epithelial-to-mesenchymal transition (EMT), migration, and invasion in U87MG cells. These results suggest that 13c is a novel inhibitor of ALK5 with potential utility in the treatment of human glioma.

© 2021 Elsevier Masson SAS. All rights reserved.

1. Introduction

Glioblastoma (GBM) is one of the most common primary malignant brain tumors, and it typically carries a poor prognosis and high mortality rates [1]. Surgical resection followed by radiotherapy with concomitant temozolomide is considered the standard treatment for GBM. Despite this multidisciplinary approach, the 5-year survival rate is only 6.8% [2]. The poor prognosis of GBM is associated with the invasiveness and metastasis of tumor cells in the normal brain [3,4].

Transforming growth factor- β (TGF- β), a 25-kDa disulfide-linked dimeric protein, exhibits high activity in aggressive gliomas [5]. Functionally, in normal epithelial cells and early-stage tumors, TGF-

β elicits tumor-suppressive effects, whereas it plays oncogenic roles in advanced gliomas [6]. This change of function is caused by the acquisition of mutations in TGF- β pathway gene, permitting escape from the TGF- β cytostatic response. In certain malignant tumors, such as gliomas, TGF- β selectively loses the ability to inhibit proliferation despite an intact the TGF- β pathway [7]. TGF- β ligands include the isoforms TGF- β 1, TGF- β 2, and TGF- β 3. Each isoform exhibits unique functions *in vivo* [8]. TGF- β ligands bind to the TGF- β type II receptor (TGF- β RII), thereby inducing TGF- β type I receptor (activin receptor-like kinase 5, ALK5) recruitment and phosphorylation [9]. The complex consisting of TGF- β RII and ALK5 then phosphorylates Smad2 and Smad3, which belong to the R-Smad protein family. Phosphorylated R-Smads are translocated to the nucleus, in which they combine with Smad4 to regulate the transcription of several genes [10–12]. Hence, it is evident that inhibition of the phosphorylation of Smad2 and Smad3 by ALK5 can block transmission of the TGF- β signal to the nucleus [13]. Small molecule inhibitors of ALK5, such as compounds 1 (SB-505124) [14], 2 (EW-7197) [15], 3 [16], 4 [17], 5 (LY-2157299) [18–20], and 6

* Corresponding author.

** Corresponding author.

E-mail addresses: jinchenghua@ybu.edu.cn, chjin2014@foxmail.com (C.H. Jin), xjjin@ybu.edu.cn (X. Jin).

¹ These authors contributed equally to this work.

[21], represent attractive modalities for controlling the TGF- β pathway, and their application in the treatment of various diseases has been reported (Fig. 1). Among these, compounds 2 (phase II) and 5 (phase II) have been approved by the US Food and Drug Administration (FDA) for the treatment of cancer, and they are currently being investigated in clinical trials for the treatment of several cancer types [13,22].

The mitogen-activated protein (MAP) kinase p38 is an important regulator of signal pathways controlling the cytokines tumor necrosis factor- α (TNF- α) [23–26] and interleukin-1 β (IL-1 β) [27,28]. The p38 MAPK family consists of four different isoforms: p38 α , p38 β , p38 γ , and p38 δ [29]. p38 α is the chief isoform implicated in inflammatory disease [30,31]. p38 α MAP kinase is activated by cellular stresses, growth factors, and cytokines (TNF- α and IL-1 β). Once activated, p38 α activates other kinases that subsequently phosphorylate heat shock proteins and transcription factors, further controlling the production of these cytokines. Furthermore, high levels of p38 α MAP kinase have been associated with non-small lung cancer [32], breast cancer [33,34], and head and neck squamous cell carcinoma (HNSCC) [35]. Therefore, p38 α MAP kinase inhibition is considered the main therapeutic strategy for preventing the production of pro-inflammatory cytokines and development of cancer. Several inhibitors targeting p38 α are being evaluated in preclinical studies and clinical trials. Among them, BIRB796, LY2228820, VX-702, and PH-797804 have been identified as highly potent inhibitors of p38 α , and they are currently under evaluation in clinical trials for inflammatory and cancer applications [31,36,37].

In recent years, many research groups have reported the activity of dual-target inhibitors in the literature and obtained good results [38–40]. In a recent study, we identified dual ALK5/p38 α MAP inhibitors possessing 3(5)-substituted-4-(quinolin-4-yl)pyrazole- and 4-(2-phenylpyridin-4-yl)pyrazoles moieties. Among these, J-1012 significantly inhibited the transcriptional activity induced by ALK5 and p38 α [41]. Moreover, the compound has exerted anti-tumor activity in colon cancer cells by inhibiting the hypoxia-inducible factor-1 α protein channel.

We previously reported that the [1,2,4]triazolo[1,5- α]pyridin-6-yl moiety of compound 2 occupies the pocket for the ATP adenine ring and forms a hydrogen bond with the NH of His283 in the backbone of the ALK5 hinge region as a hydrogen acceptor [15,42]. We assumed that groups containing hydrogen bond donors are introduced into the 4-position of the central imidazole ring in compound 2, and these groups may form hydrogen bonds with the carbonyl group of His283, thereby improving the inhibitory activity against ALK5. To test this assumption, we introduced an indazolyl moiety instead of [1,2,4]triazolo[1,5- α]pyridine at the 4-position of the imidazole in compound 2, thereby generating compounds 13a–g. To compare the effects of compounds containing hydrogen bond donors with those containing acceptors against ALK5, the methylated indazolyl-derived imidazoles 20a–g were also designed (Fig. 2).

2. Results and discussion

2.1. Chemistry

The reaction sequence for the synthesis of the seven new imidazole derivatives 13a–g is outlined in Scheme 1. Lithiation of 5-bromo-1H-indazole (7) with *n*-BuLi at -50 °C in tetrahydrofuran (THF), followed by treatment with anhydrous dimethylformamide (DMF) to afford 1H-indazole-5-carbaldehyde (8) at a yield of 58% [43]. The aldehyde 8 was coupled with diphenyl (6-methylpyridin-2-yl)(phenylamino)methylphosphonate [44] in a mixture of THF and *i*-PrOH in the presence of C_2CO_3 at room temperature, followed by treatment with 1 N HCl to afford ketone 2-(1H-indazol-5-yl)-1-(6-methylpyridin-2-yl)ethanone (9) in a 58% yield [13]. Oxidation of compound 9 with 40% HBr in dimethyl sulfoxide (DMSO) led to diketone 10 in a 44% yield [44,45]. Cyclization of diketone 10 with 60% 2,2-dimethoxyacetaldehyde in H_2O and NH_4OAc in a mixture of *t*-BuOMe and MeOH at 50 °C gave imidazole 11 at a yield of 64% [15]. Hydrolysis of compound 11 in 1 N HCl solution at 70 °C afforded imidazole-2-carboxaldehyde 12 at a yield of 96%. To observe the effect of substituents on the activity of

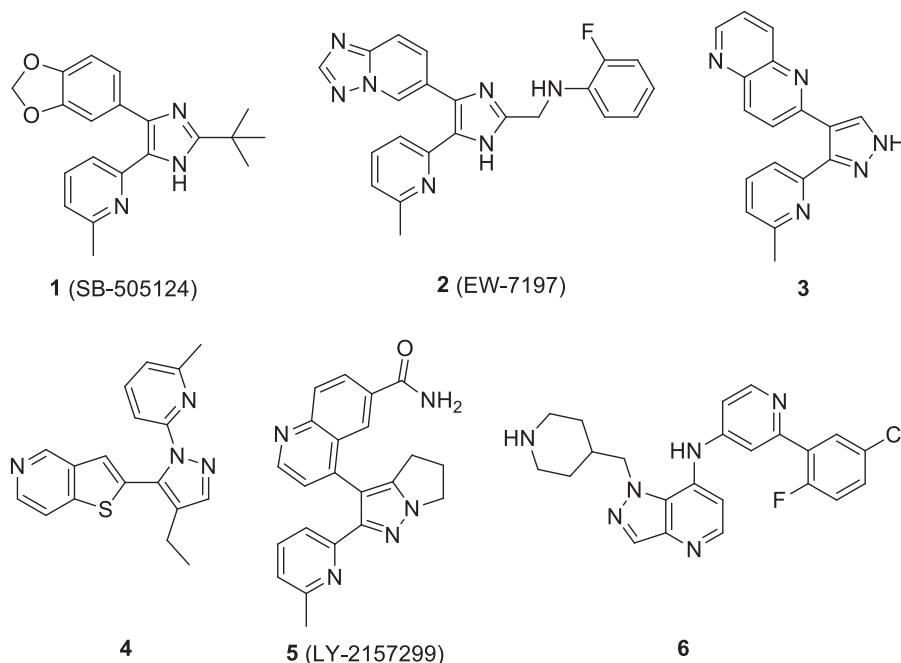


Fig. 1. Presentative classical ALK5 inhibitors.

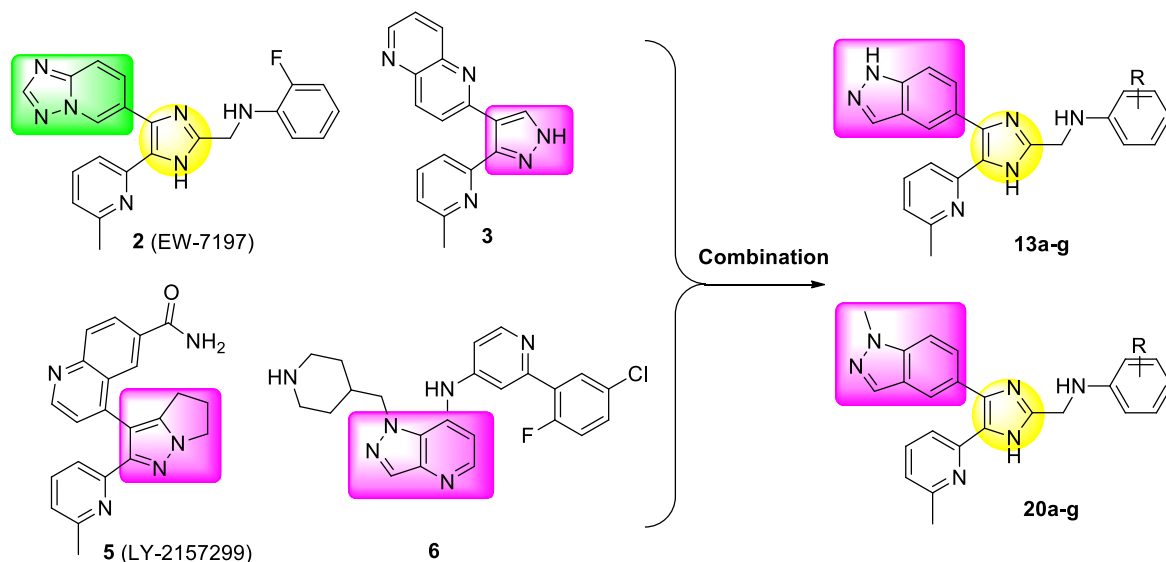
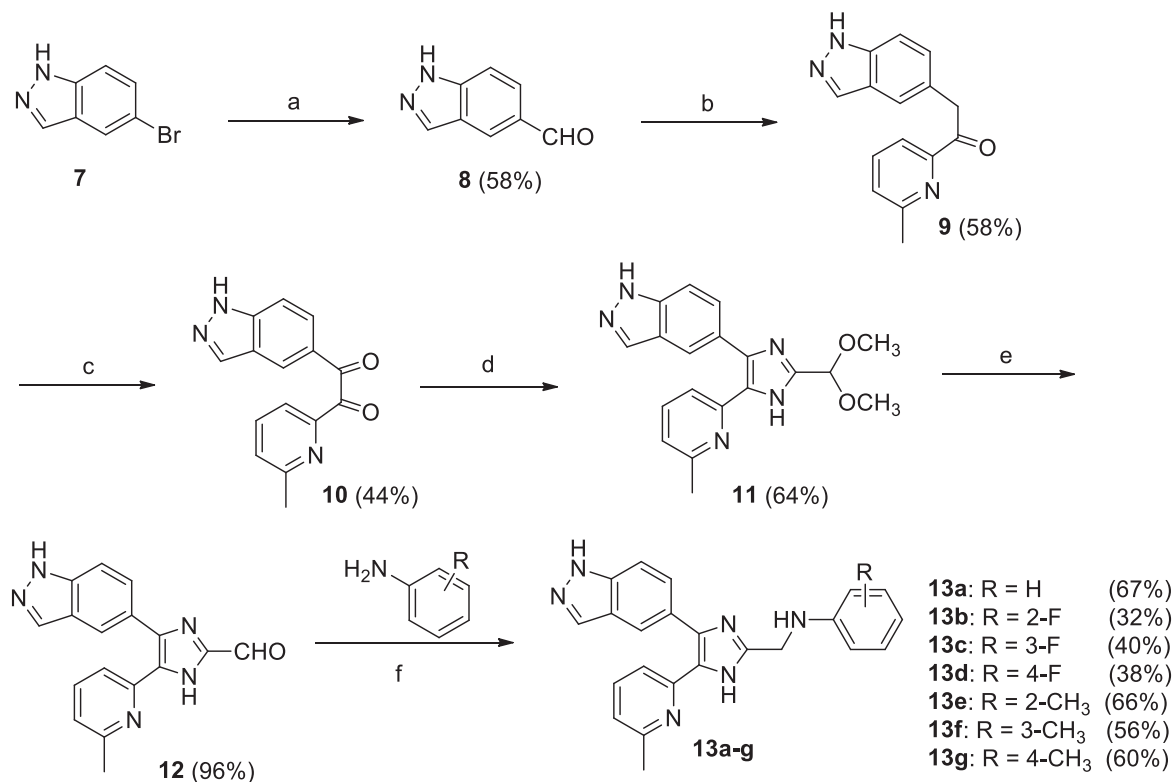


Fig. 2. The design strategy based on compounds 2, 3, 5 and 6.

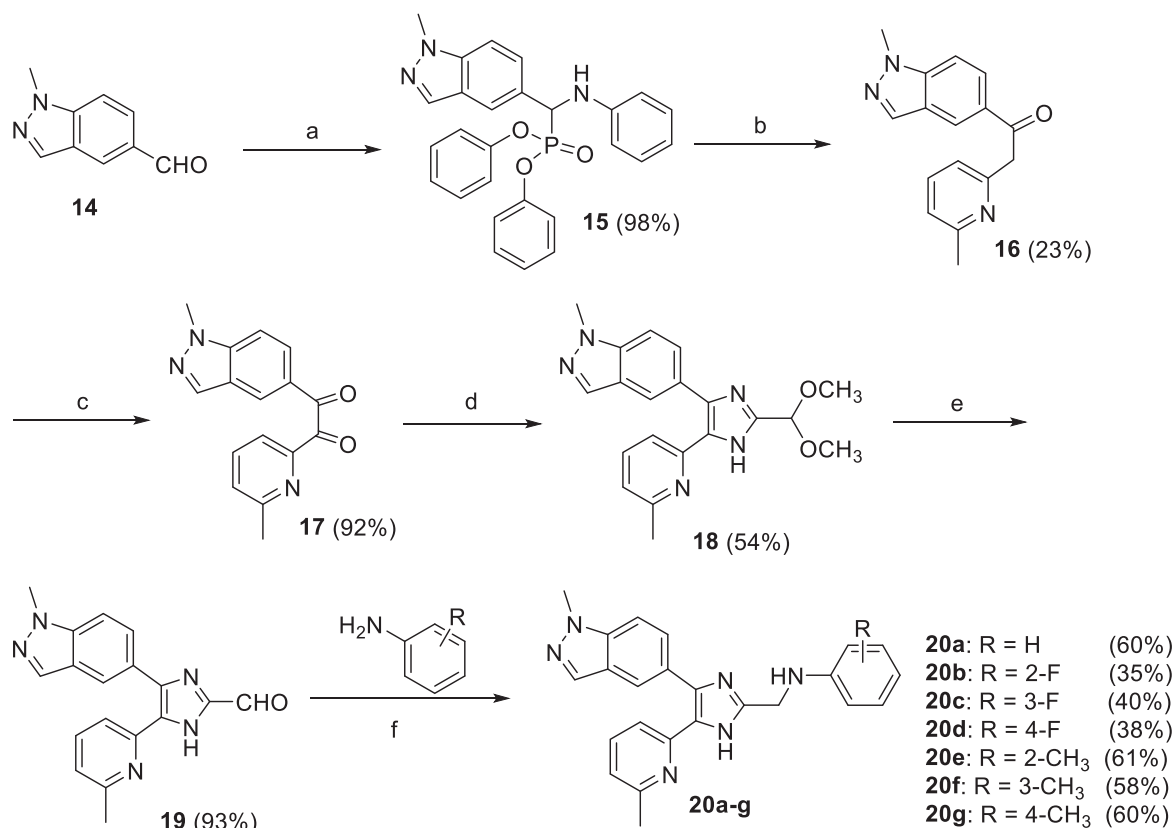


Scheme 1. Synthesis of compounds 13a–g. Reagents and conditions: (a) i) *n*-BuLi (1.6 M in hexane), THF, $-50\text{ }^{\circ}\text{C}$, 2 h; ii) anhydrous DMF, $-50\text{ }^{\circ}\text{C}$, 0.5 h; (b) i) diphenyl (6-methylpyridin-2-yl)(phenylamino)methylphosphonate, Cs_2CO_3 , THF: *i*-PrOH (4:1), rt, 12 h; ii) 1 N HCl, 1 h; (c) 40% HBr in H_2O , DMSO, $70\text{ }^{\circ}\text{C}$, 1.5 h; (d) 60% 2,2-dimethoxyacetaldehyde in H_2O , NH_4OAc , MeOH (1:1), $50\text{ }^{\circ}\text{C}$, 2 h; (e) 1 N HCl, $70\text{ }^{\circ}\text{C}$, 4 h; (f) (i) AcOH, 1,2-dichloroethane, $75\text{ }^{\circ}\text{C}$, 2 h; (ii) NaBH_4 , MeOH, rt, 3 h.

aromatic rings on the side chain, coupling of the 12 with appropriately substituted anilines in 1,2-dichloroethane in the presence of AcOH at $75\text{ }^{\circ}\text{C}$, followed by reduction of the resulting imines with NaBH_4 in MeOH to give the target compounds 13a–g at yields of 32%–67% [13].

To compare the effect of the indazole hydrogen and its replacement on activity, the 4-(1-methyl-1H-indazol-5-yl)-5-(6-

methylpyridin-2-yl)-1H-imidazoles 20a–g were synthesized as presented in Scheme 2. 1-Methyl-1H-indazole-5-carbaldehyde (14) was treated with aniline and diphenyl phosphite in *i*-PrOH at room temperature to afford diphenyl ((1-methyl-1H-indazol-5-yl)(phenylamino)methyl)phosphonate (15) in a 98% yield [46]. Coupling of the 15 with 6-methylpyridine-2-carboxaldehyde in a mixture of THF and *i*-PrOH at room temperature in the presence



Scheme 2. Synthesis of compounds 20a–g. Reagents and conditions: (a) aniline, diphenyl phosphite, *i*-PrOH, rt, 3 h; (b) i) 6-methylpyridine-2-carboxaldehyde, Cs₂CO₃, THF: *i*-PrOH (4:1), rt, 24 h; ii) 1 N HCl, 1 h; (c) 40% HBr in H₂O, DMSO, 70 °C, 1.5 h; (d) 60% 2,2-dimethoxyacetaldehyde in H₂O, NH₄OAc, *t*-BuOMe: MeOH (1:1), 50 °C, 2 h; (e) 1 N HCl, 70 °C, 4 h; (f) (i) AcOH, 1,2-dichloroethane, 75 °C, 2 h; (ii) NaBH₄, MeOH, rt, 3 h.

of Cs₂CO₃, followed by hydrolysis with 1 N HCl to give the monoketone 16 at a yield of 23% [46]. Target compounds (20a–g) were synthesized from compound 16 in four steps using the same synthetic route and reaction conditions described in Scheme 1.

2.2. Biological evaluation

2.2.1. Inhibition of ALK5 kinase activity by the compounds

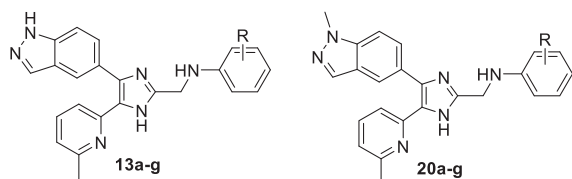
To investigate whether compounds 13a–g and 20a–g could inhibit ALK5 activity, their half-maximal inhibitory concentrations (IC₅₀s) were measured. To observe the influence of substituents on the ALK5 inhibitory activity of the benzene rings on the side chain, we introduced electron-withdrawing and electron-donating groups, such as fluorine atoms and methyl groups, into the *ortho*, *meta*, or *para* position of the benzene ring. Compounds 5 (LY-2157299) and 2 (EW-7197) were used as positive controls. We anticipated that inserting hydrogen bond donors at the 4-position of the imidazole moiety in compound 2 would improve the binding affinity of the nitrogen atom for ALK5 related proteins, and further enhance its ALK5 inhibitory activity. All compounds possessing 1*H*-indazol-5-yl (13a–g) and 1-methyl-1*H*-indazol-5-yl (20a–g) moieties exhibited 3.8–32.3-fold more potent ALK5 inhibition (IC₅₀ = 0.004–0.034 μM) than compound 5 (IC₅₀ = 0.129 μM; Table 1). Compounds 13a–g more potently inhibited ALK5 activity (IC₅₀ = 0.004–0.009 μM) than compound 2 (IC₅₀ = 0.014 μM). These results illustrated that among compounds 13 types, the inserting electron-withdrawing (F) and electron-donating groups (CH₃) into the benzene ring increased their ability to inhibit ALK5,

but the effect of substituents was not evident. Among compound 20 types, all compounds (20a–g; IC₅₀ = 0.010–0.024 μM) excluding compound 20 g (IC₅₀ = 0.034 μM) exhibited similar ALK5 inhibitory activity as the positive control compound 2. These data demonstrated that among compound 20 types, both electron-withdrawing and electron-donating groups at the *ortho* or *meta* position of the benzene ring increased ALK5 inhibition; by contrast, an electron-withdrawing group (20d, IC₅₀ = 0.016 μM) resulted in better ALK5 inhibitory activity than the electron-donating group at the *para* position on the benzene ring. Between the two compound series, compounds 13a (IC₅₀ = 0.004 μM) and 13c (IC₅₀ = 0.004 μM) most potently inhibited ALK5, displaying 32.3- and 3.5-fold greater inhibitory activity than compounds 5 and 2, respectively. As expected, the results revealed that an indazolyl group introduced at the 4-position of the imidazole moiety in compound 2 appeared to be accommodated favorably into the ATP-binding pocket of ALK5, potentiating its ALK5 inhibitory activity. In addition, the results highlighted that introduction of a methylated indazolyl group resulted in weaker ALK5 inhibition than insertion of an indazolyl group at the same position in compound 2, which may be attributable to steric hindrance.

2.2.2. Inhibition of p38α MAP kinase activity by the compounds

In previous studies, we used p38α MAP kinase as a selective kinase relative to ALK5 because its kinase domain is considered most similar to that of ALK5 [13]. Unlike previous finding [13,15,42], compounds 13a–g and 20a–g exhibited good p38α MAP inhibitory activity (IC₅₀ = 0.004–0.565 μM; Table 1). In the two series, all compounds (IC₅₀ = 0.004–0.052 μM) of series 13 excluding

Table 1
Inhibitory activity of 4-(1H-indazol-5-yl)-5-(6-methylpyridin-2-yl)-1H-imidazoles **13a–g** and 4-(1-methyl-1H-indazol-5-yl)-5-(6-methylpyridin-2-yl)-1H-imidazoles **20a–g** on ALK5 and p38 α .fx1



Compound	R	IC ₅₀ (μM)	
		p38 α ^a	ALK5 ^b
13a	H	0.013 ± 0.0008	0.004 ± 0.0006
13b	2-F	0.020 ± 0.0005	0.005 ± 0.0003
13c	3-F	0.004 ± 0.0006	0.004 ± 0.0004
13d	4-F	0.052 ± 0.0010	0.006 ± 0.0008
13e	2-CH ₃	0.023 ± 0.0003	0.005 ± 0.0005
13f	3-CH ₃	0.032 ± 0.0007	0.008 ± 0.0006
13g	4-CH ₃	0.329 ± 0.0021	0.009 ± 0.0008
20a	H	0.066 ± 0.0003	0.014 ± 0.0003
20b	2-F	0.095 ± 0.0004	0.013 ± 0.0007
20c	3-F	0.026 ± 0.0005	0.011 ± 0.0007
20d	4-F	0.112 ± 0.0009	0.016 ± 0.0004
20e	2-CH ₃	0.071 ± 0.0006	0.024 ± 0.0005
20f	3-CH ₃	0.023 ± 0.0003	0.010 ± 0.0006
20g	4-CH ₃	0.565 ± 0.0015	0.034 ± 0.0007
5 (LY-2157299)		0.493 ± 0.0005	0.129 ± 0.0004
2 (EW-7197)		2.950 ± 0.0004	0.014 ± 0.0003

^{a,b}Values are the average of three independent experiments run in triplicate.

^a p38 α MAP kinase was expressed in *E. coli* as untagged human recombinant protein.

^b ALK5 was expressed in Sf9 insect cells as a human recombinant GST-fusion protein using the baculovirus expression system.

compound **13g** (IC₅₀ = 0.329 μM) strongly inhibited p38 α MAP activity, whereas all compounds (IC₅₀ = 0.066–0.565 μM) of series **20** excluding compounds **20c** (IC₅₀ = 0.026 μM) and **20f** (IC₅₀ = 0.023 μM) moderately inhibited p38 α MAP activity. Between the two compounds series, compound **13c** (IC₅₀ = 0.004 μM) mostly strongly inhibited p38 α MAP kinase activity, displaying 123.3- and 737.5-fold greater inhibitory activity than compounds **5** (IC₅₀ = 0.493 μM) and **2** (IC₅₀ = 2.950 μM), respectively.

2.2.3. Docking study

2.2.3.1. Docking of compounds **13c** and **20g** in the ALK5 active site.

To rationalize the structure-activity relationship (SAR) shown in [Table 1](#), we examined the binding modes of two representative ligands from two series of compounds, **13c** and **20g**, using the semi-flexible molecular docking programs Libdock [47]. Docking analyses were performed using the recently reported X-ray structure of ALK5 in complex with a pyrazole ALK5 inhibitor (PDB: 1RWB) [48]. As expected, the carbonyl group of His283 formed hydrogen bond with the NH group of 1H-indazol-5-yl moiety in **13c** and a hydrogen atom of Tyr282 formed hydrogen bond with the nitrogen atom of 1H-indazol-5-yl moiety in **13c**, respectively ([Fig. 3A](#) and [B](#)). The fluoride atom on benzene ring of side chain in **13c** formed a hydrogen bond and a halogen bond with amine on the side chain of Lys335 and the carbonyl group on the side chain of Asn338, respectively. The amine group on the side chain in **20g** formed a hydrogen bond with the carbonyl group of Lys337 ([Fig. 3C](#) and [D](#)). The central imidazole ring in **20g** formed an unfavorable donor-donor bond with the amine group on the side chain of Lys232. The pyridine moiety of **13c** and 1-methyl-1H-indazol-5-yl moiety of **20g** were stretched to the back of the hydrophobic pocket.

Compound **13c** showed higher ALK5 inhibitory activity than compound **20g**, which may be related to the following two reasons. Not only calculated binding energy scores (LibDock Score) of these two compounds indicated that **13c** (−144.272 kcal/mol) formed more stable complexes with ALK5 than did **20g** (−134.707 kcal/mol), but also compound **13c** (His283, Tyr282, Lys335, and Asn338) showed more bonding with previously reported key amino acids than did compound **20g** (Lys337 and Lys232) [22,49]. Furthermore, compound **13c** seemed to be more favorably accommodated in the binding pocket of ALK5 than compound **20g**.

2.2.3.2. Docking of compound **13c** in the p38 α active site.

Compound **13c** showed the highest inhibitory activity in p38 α MAP analysis ([Table 1](#)). In an attempt to explore the binding affinity of **13c** in the p38 α active site, the binding mode was investigated through a molecular docking study [50,51]. Fluoride atom on the benzene ring of side chain in **13c** formed a hydrogen bond with Thr106 ([Fig. 4A](#)). It was shown that the pyridine moiety of **13c** was stretched into the back of the binding pocket of p38 α consisting of Leu74, Leu75, Phe169, Glu71, Asp168, Ile84, Lys53, Thr106, Als51, Ala172, Arg67, and Arg173 ([Fig. 4B](#)). We found that compound **13c** did not form any bonds with Ser280. As bonding with Ser280 is known to be vital for the selectivity of ligands toward ALK5 over p38 α MAP kinase, this may be the reason for the low selectivity of these two series compounds [41]. High selectivity to different kinases leads to lower toxicity of compounds. This part was identified in our lead compound studies [15]. As anti-tumor drugs, dual-target inhibitors have synergistic effects. In fact, these results indicate that compound **13c** has a good binding affinity with p38 α -related proteins.

2.2.4. **13c** inhibits the expression and nuclear translocation of slug in TGF- β -stimulated U87MG cells

TGF- β is one of the most well-known inducers of epithelial-to-mesenchymal transition (EMT) in late-stage cancers [52]. EMT is a cellular process associated with various tumor functions [53], and it is often defined by the loss of the epithelial cell adhesion protein E-cadherin together with the gain of the mesenchymal-associated molecules N-cadherin and vimentin [54–56]. Numerous studies revealed that EMT plays an important role in tumor progression, and it is an essential factor for the invasion and migration of tumor cells [55,57]. TGF- β signaling also promotes the expression of EMT-related gene, such as Snail1, Snail2, ZEB1, ZEB2, and LEF1, which accelerate the loss of cell–cell adhesion and cytoskeletal rearrangement [58].

Slug (Snail2), a member of the Snail family, downregulates E-cadherin transcription with the E-box elements in EMT progression [59]. Studies have indicated that Slug expression is correlated with tumor biological aggressiveness [60,61]. Both Snail1 and Snail2 are associated with increased invasion and migration of malignant gliomas [62].

To observe the ETM inhibitory activity of the synthesized compounds, the compound with the highest activity, **13c** (J-1090), was selected. Initially, the effects of compounds **13c** and **5** Slug protein expression in TGF- β -stimulated U87MG cells were evaluated. Western blot analysis revealed that **13c** treatment significantly suppressed Slug protein expression in a concentration-dependent manner in U87MG cells ([Fig. 5A](#), lanes 5 and 6). Interestingly, compound **13c** more strongly suppressed Slug expression than compound **5** ([Fig. 5A](#), lanes 3–6). We next evaluated the effect of **13c** on the nuclear translocation of Slug in U87MG cells using immunofluorescence assays. The results indicated that in cells treated with TGF- β alone, Slug translocated to the nucleus, whereas in cells pretreated with **13c** (1 μM) followed by TGF- β exposure, the nuclear translocation of Slug was significantly inhibited ([Fig. 5B](#)).

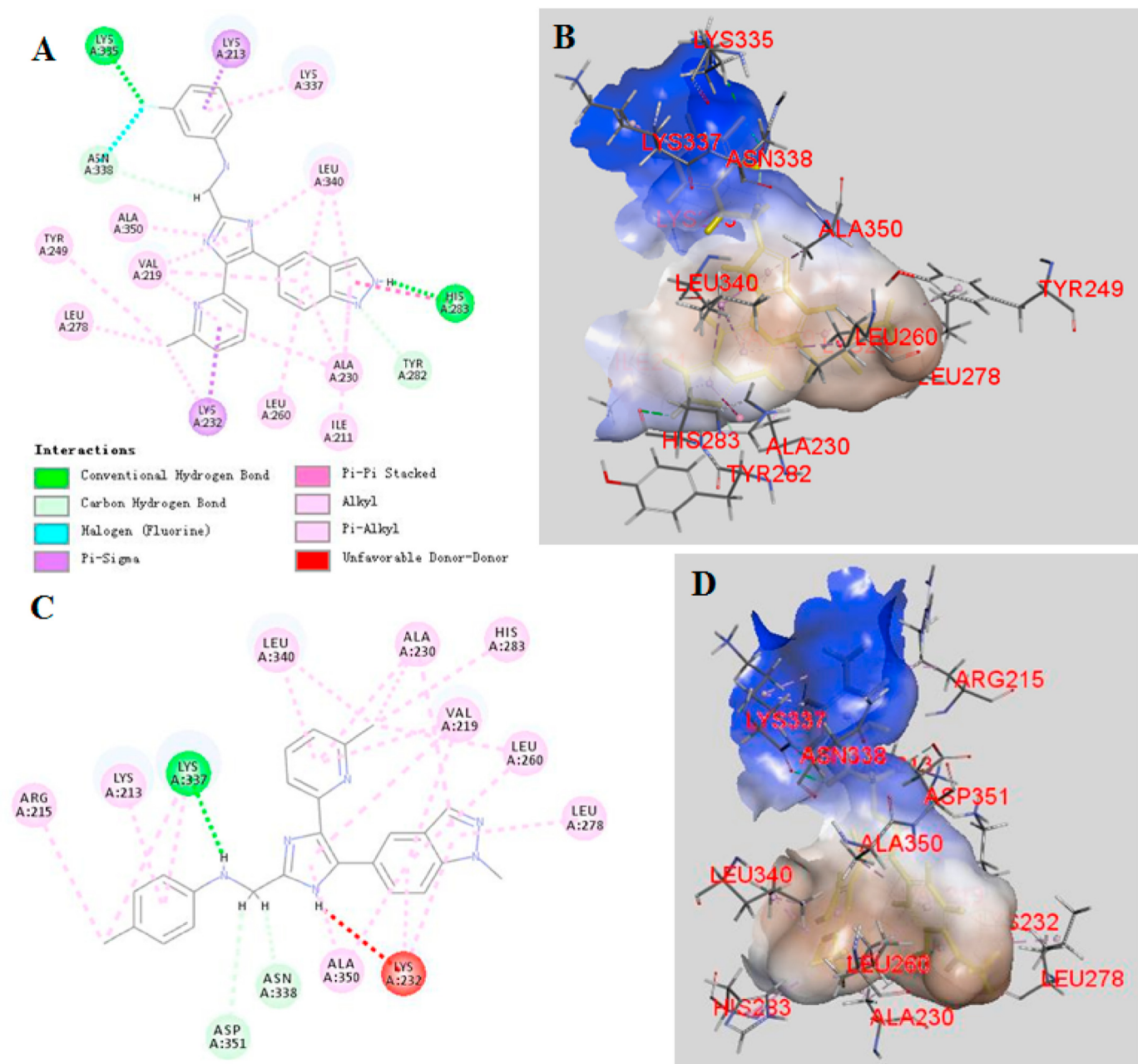


Fig. 3. Docking conformation of compounds 13c and 20g in the active site of ALK5 (PDB: 1RWB). (A) 2D binding model of 13c. (B) Proposed conformation of 13c in the binding pocket of ALK5. (C) 2D binding model of 20g. (D). Proposed conformation of 20g in the binding pocket of ALK5. Lipophilicity increases from blue (hydrophilic) to brown (lipophilic). The ligands are shown in yellow.

2.2.5. 13c blocks TGF- β -induced morphological changes

Previous studies demonstrated that TGF- β overexpression promotes morphological changes and EMT in cancer cells [63]. We then explored whether compound 13c impedes TGF- β -induced morphological changes in U87MG cells. After a single treatment for 48 h, TGF- β induced elongation characteristic of EMT in U87MG cells. However, 13c treatment inhibited this morphological change. We also found that concomitant treatment with compound 13c more strongly prevented this change than 5 in TGF- β -treated U87MG cells (Fig. 6). These data suggested that 13c can induce EMT reversal.

2.2.6. 13c reverses EMT induced by TGF- β

To determine whether 13c reverses TGF- β -induced EMT, we first assessed the expression of N-cadherin, a mesenchymal marker, in U87MG cells treated with 13c in the presence or absence of TGF- β . Immunofluorescence assays revealed that 13c reversed the upregulation of N-cadherin induced by TGF- β (Fig. 7A). Next, we further examined the reversal of EMT under 13c treatment through an examination of the protein and mRNA levels of EMT markers via western blotting and RT-PCR. As anticipated, the presence of 13c decreased the TGF- β -stimulated expression of N-cadherin and vimentin at both the protein and mRNA levels (Fig. 7B and C).

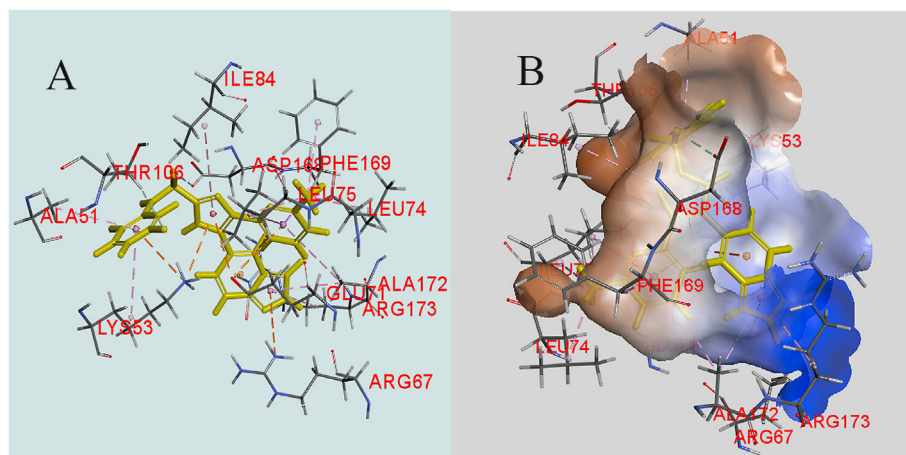


Fig. 4. Docking conformation of compound 13c in the active site of p38 α (PDB: 1A9U). (A) 3D binding model of 13c. (B) Proposed conformation of 13c in the binding pocket of p38 α . Lipophilicity increases from blue (hydrophilic) to brown (lipophilic). The ligand is shown in yellow.

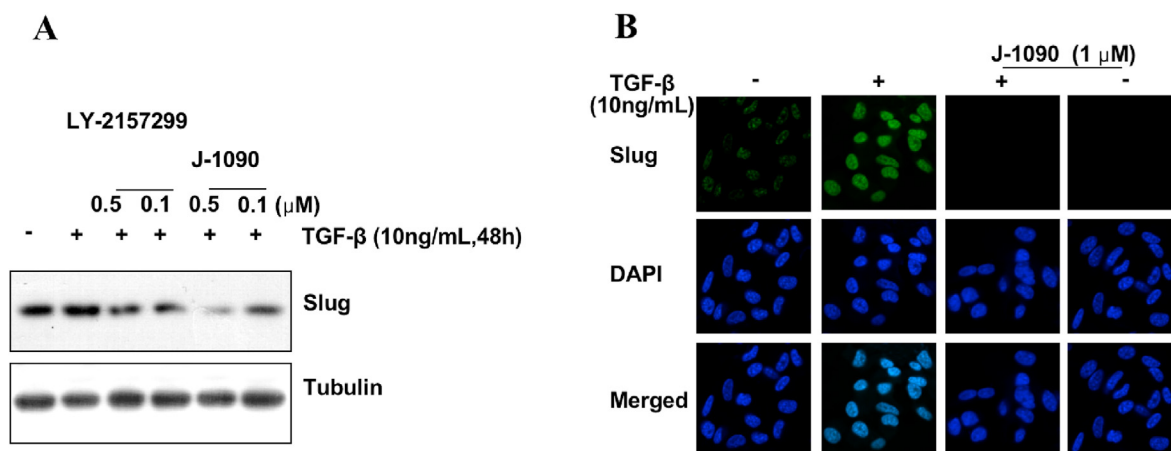


Fig. 5. 13c (J-1090) inhibition of expression and nuclear translocation of Slug *in vitro*. (A) Western blots to assess protein levels of Slug after treatment with TGF- β (10 ng/mL) in the presence of 13c or 5 (LY-2157299). (B) Control and TGF- β -stimulated U87MG cells were treated with or without 13c for 48 h. After fixation, cells were incubated with anti-Slug (1:200) and fluorescence was visualized by Alexa fluor[®] 488 goat anti-mouse IgG (H + L). Nuclei were stained with 4',6-diamidino-2-phenylindole (DAPI).

Intriguingly, 13c more strongly suppressed EMT marker suppression than 5 (Fig. 7B).

2.2.7. 13c inhibits the increased migration and invasion induced by TGF- β

It has been documented that TGF- β plays a crucial role in promoting cancer cell migration and invasion. To examine the influence of compound 13c on TGF- β -induced motility of U87MG cells, we performed wound-healing and Matrigel invasion assays. The results illustrated that wound closure and cell invasion were significantly accelerated by TGF- β , whereas 13c completely inhibited these effects of TGF- β on cell migration and invasion (Fig. 8A and B).

TGF- β is an important cytokine in embryogenesis and tissue homeostasis [63]. TGF- β plays a dual and opposite role in tumorigenesis. TGF- β is known to inhibit cell growth via G1 arrest during the cell cycle and apoptosis of normal and premalignant cells, whereas this cytokine can promote tumor progression and metastasis in advanced cancer. Tumor cells escape the growth inhibitory effect of TGF- β by selectively damaging the anti-tumor response [63,64]. In the second case, several pathways triggered by TGF- β were controlled by cancer cells, transforming TGF- β into

an oncogenic gene that induces immunosuppression, angiogenesis, migration, and invasion. TGF- β has been revealed to promote the EMT process by regulating the EMT transcription factor Slug. Targeting TGF- β during EMT may provide a potential strategy for cancer treatment. Recent studies illustrated that TGF- β inhibition can reverse treatment resistance, enhance the synergy of combination regimens, and increase sensitivity to radiotherapy in cell and mouse models [63]. To inhibit TGF- β signal transduction, several small- and large-molecule compounds have been developed, but a full understanding of the biology of TGF- β in cancer is needed to guarantee the development of effective treatments and prevent adverse side effects.

3. Conclusion

In this report, a series of 4-(1*H*-indazol-5-yl)-5-(6-methylpyridin-2-yl)-1*H*-imidazoles 13a–g and a series of 4-(1-methyl-1*H*-indazol-5-yl)-5-(6-methylpyridin-2-yl)-1*H*-imidazoles 20a–g were synthesized and evaluated for their inhibitor effects on ALK5 and p38 α MAP kinase activities in enzymatic assays. We discovered that the insertion of 1*H*-indazol-5-yl and 1-methyl-1*H*-indazol-5-yl moieties at the 4-position of the imidazole ring

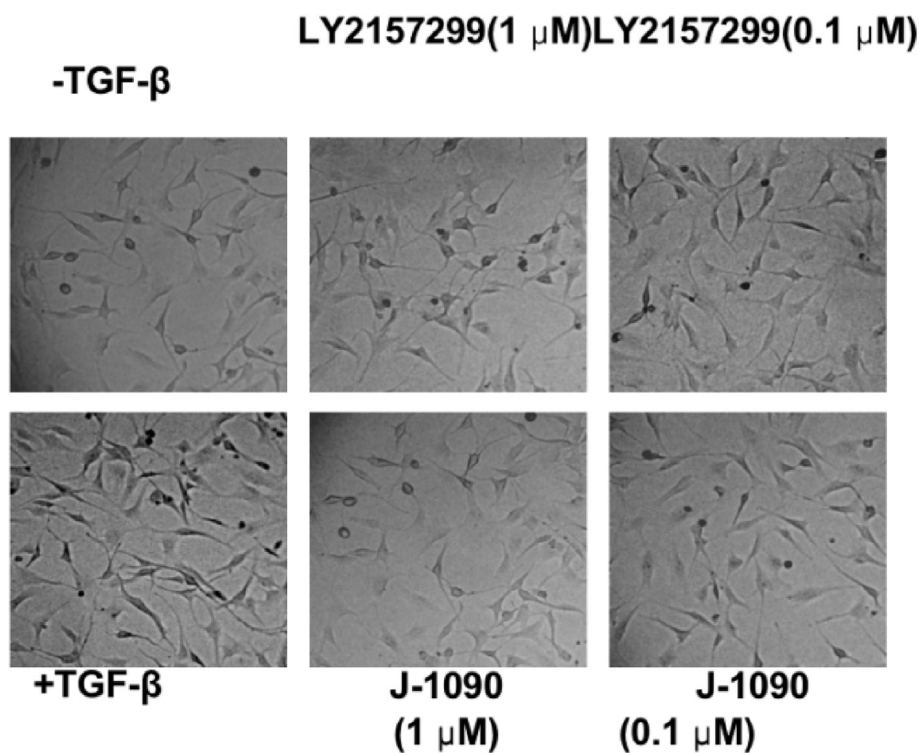


Fig. 6. Morphology of U87MG cells before and after stimulation with TGF- β , or stimulation in the presence of 13c or 5 (LY-2157299) for 48 h.

significantly increased ALK5 and p38 α inhibitory activities of the compounds. The most potent compound, 13c, inhibited ALK5 with an IC₅₀ of 0.004 μ M in the enzymatic assay, which was 32.3- and 3.5-fold more potent than positive controls 5 and 2, respectively. Compound 13c (IC₅₀ = 0.004 μ M) also exhibited the greatest inhibitory activity against p38 α MAP kinase, suppressing its activity by 123.3- and 737.5-fold compared with effects of compounds 5 (IC₅₀ = 0.493 μ M) and 2 (IC₅₀ = 2.950 μ M), respectively. The molecular docking results highlighted that groups possessing hydrogen bond donors at the 4-position in 1-substituted-3-(6-methylpyridin-2-yl)imidazoles may be important for good ALK5 inhibition. Compound 13c (J-1090) could inhibit TGF- β -induced invasion and metastasis. This effect appears to be produced by the promotion of TGF- β -induced activation and EMT progression. Furthermore, our results suggest that 13c, a novel inhibitor of ALK5, inhibited EMT, motility, and invasiveness in glioma cells *in vitro*.

4. Experimental section

4.1. Chemistry

All commercially available reagents were obtained from Aladdin (Shanghai, China). In general, all reactions were performed under normal atmosphere and at room temperature unless otherwise noted. Melting points were measured in open glass capillaries tube in an electrical melting point (B-540, Büchi) and are uncorrected. ¹H and ¹³C NMR spectra were recorded on Bruker NMR spectrometers at 300 MHz and 500 MHz, respectively, tetramethylsilane (TMS) was used as internal standard. Chemical shifts were signified in ppm (δ) relative to internal TMS in CDCl₃, CDCl₃/CD₃OD, or DMSO-*d*₆ and coupling constants (*J*) are in hertz (Hz). ¹⁹F NMR spectra were recorded on Bruker NMR spectrometers at 470 MHz. High resolution mass spectra electrospray ionization (HRMS-ESI) was obtained on a Thermo Scientific LTQ Orbitrap XL spectrometer

(Thermo Fisher Scientific, USA). The purity of the tested compounds was determined using an Agilent 1260 series HPLC system using a C₁₈ column (packing ODS HG 5 μ M, 4.6 \times 250 mm), and that for all the compounds was found to be >96%.

4.1.1. Synthesis of 1H-indazole-5-carbaldehyde (8)

To a solution of 5-bromo-1H-indazole (7, 6.00 g, 30.46 mmol) in tetrahydrofuran (THF, 120 mL) at -50 °C under nitrogen, a solution of *n*-butyllithium (1.6 M in hexane, 48 mL, 76.15 mmol) was added dropwise, and the mixture was continuously stirred for 2 h. To it, anhydrous dimethylformamide (DMF, 4.7 mL, 60.92 mmol) was added and stirred for 30 min. The reaction mixture was quenched with water, and the mixture was allowed to room temperature. The mixture was extracted with ethyl acetate (3 \times 120 mL) and the organic layer was combined. The organic layer was washed with brine, dried over anhydrous Na₂SO₄, filtered, and then evaporated to dryness under reduced pressure. The residue was purified by column chromatography on silica gel using Petroleum ether and ethyl acetate (4:1) as eluent to give the titled compound 8 as a solid.

Yellow solid; Yield 58%; ¹H NMR (300 MHz, CDCl₃) δ 10.54 (br s, 1H, NH), 10.07 (s, 1H), 8.32 (s, 1H), 8.27 (s, 1H), 7.99 (d, 1H, *J* = 9.0 Hz), 7.62 (d, 1H, *J* = 9.0 Hz).

4.1.2. Synthesis of 2-(1H-indazol-5-yl)-1-(6-methylpyridin-2-yl) ethanone (9)

To a stirred solution of compound 8 (5.20 g, 35.58 mmol) in a mixture of THF (80 mL) and *i*-PrOH (20 mL), diphenyl (6-methylpyridin-2-yl)(phenylamino)-methylphosphonate (20.00 g, 46.25 mmol) and Cs₂CO₃ (15.00 g, 46.25 mmol) were added. The mixture was stirred at room temperature for 12 h, and to it, 1 N HCl (150 mL) was added dropwise about 30 min and stirred for additional 1 h. The reaction mixture was diluted with MTBE (75 mL). The aqueous layer was separated and neutralized with saturated NaHCO₃ solution at 0 °C. The aqueous layer was extracted with

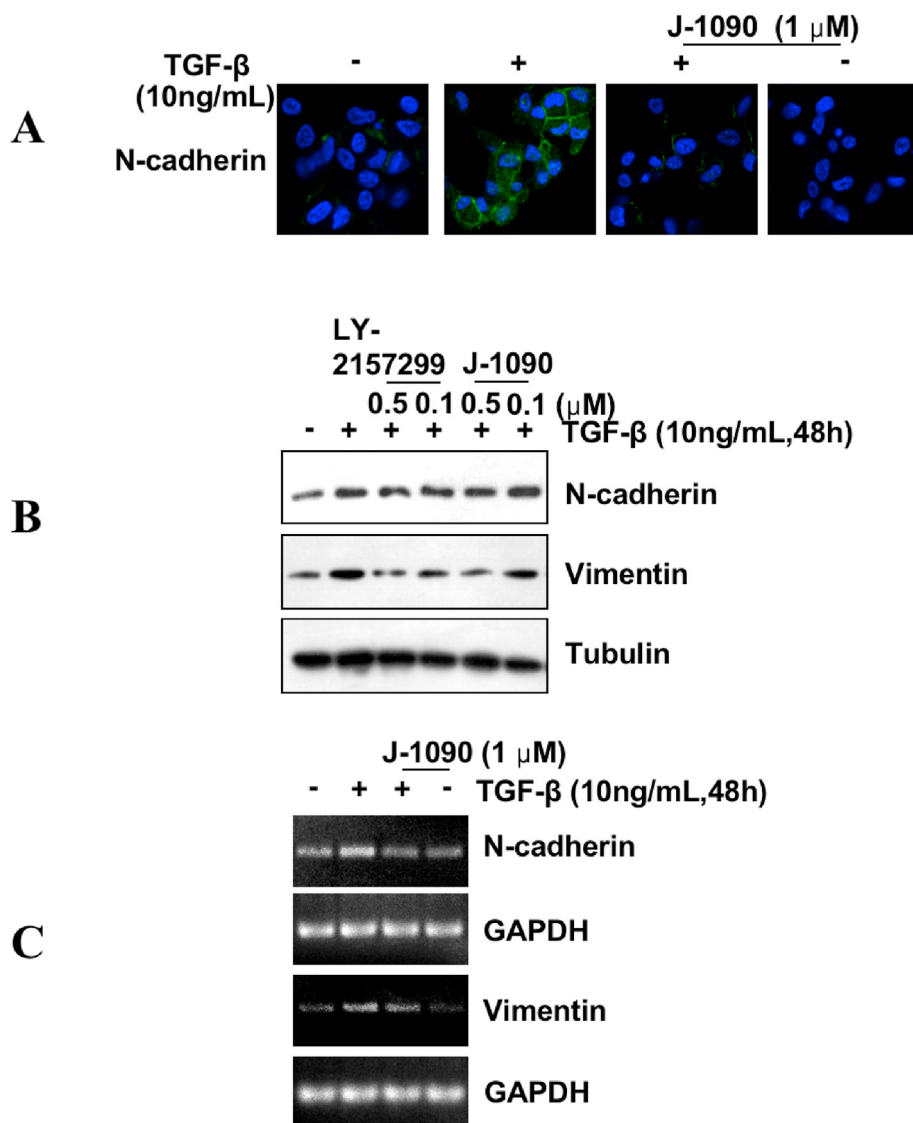


Fig. 7. 13c (J-1090) reverses EMT in U87MG cells. (A) Vehicle and TGF- β -stimulated U87MG cells were treated with or without 13c for 48 h. After fixation, cells were incubated with anti-N-cadherin (1:200) and fluorescence was visualized by Alexa fluor[®] 488 goat anti-mouse IgG (H + L). Nuclei were stained with 4',6-diamidino-2-phenylindole (DAPI). (B) U87MG cells were treated with TGF- β (10 ng/mL) in the presence of 13c or 5 (LY-2157299) for 48 h. The protein levels of N-cadherin and Vimentin were measured by western blot analysis. (C) U87MG cells were treated with TGF- β (10 ng/mL) in the presence of 13c or 5 for 48 h. The mRNA levels of N-cadherin and Vimentin were measured by RT-PCR.

ethyl acetate (3 x 120 mL). The combined organic layer was washed with brine, dried over anhydrous Na₂SO₄, filtered, and then evaporated to dryness under reduced pressure. The residue was purified by column chromatography on silica gel using Petroleum ether and ethyl acetate (5:1) as eluent to give the titled compound 9 as a solid.

White needle solid; Yield 58%; ¹H NMR (300 MHz, DMSO-*d*₆) δ 13.01 (br s, 1H, NH), 8.00 (s, 1H), 7.89 (t, 1H, *J* = 7.5 Hz), 7.78 (d, 1H, *J* = 6.0 Hz), 7.63 (s, 1H), 7.55 (d, 1H, *J* = 9.0 Hz), 7.47 (d, 1H, *J* = 9.0 Hz), 7.27 (d, 1H, *J* = 9.0 Hz), 4.58 (s, 2H), 2.63 (s, 3H).

4.1.3. Synthesis of diphenyl ((1-methyl-1H-indazol-5-yl)(phenylamino)methyl)- phosphonate (15)

To a mixture of 1-methyl-1H-indazole-5-carbaldehyde (14, 4.50 g, 28.10 mmol) and aniline (3.08 mL, 33.72 mmol) in *i*-PrOH (45 mL), diphenyl phosphite (8.55 mL, 44.72 mmol) was added. The mixture was stirred at room temperature for 3 h, and then it cooled to 0 °C and stirred for additional 45 min. The precipitates were collected by filtration using a Büchner funnel and dried in a vacuum oven to gain the compound 15 as a solid.

Yellow solid; Yield 98%; ¹H NMR (300 MHz, CDCl₃) δ 7.92 (s, 1H), 7.90 (s, 1H), 7.60 (d, 1H, *J* = 9.0 Hz), 7.37 (d, 1H, *J* = 9.0 Hz), 7.30–7.25 (m, 2H), 7.20–7.08 (m, 8H), 6.88 (d, 2H, *J* = 9.0 Hz), 6.73 (t, 1H, *J* = 7.5 Hz), 6.64 (d, 2H, *J* = 9.0 Hz), 5.25 (d, 1H, *J* = 24.0 Hz), 4.93 (br s, 1H), 4.05 (s, 3H).

4.1.4. Synthesis of 1-(1-methyl-1H-indazol-5-yl)-2-(6-methylpyridin-2-yl)ethanone (16)

To a stirred solution of 6-methylpyridine-2-carboxaldehyde (2.6 g, 21.46 mmol) in a mixture of THF (120 mL) and *i*-PrOH (30 mL), compound 9 (13.15 g, 28.01 mmol) and Cs₂CO₃ (9.13 g, 28.01 mmol) were added. The mixture was stirred at room temperature for 24 h, and to it, 1 N HCl (90 mL) was added dropwise about 20 min and stirred for additional 1 h. The reaction mixture was diluted with MTBE (45 mL). The aqueous layer was separated and neutralized with saturated NaHCO₃ solution at 0 °C. The aqueous layer was extracted with ethyl acetate (3 x 50 mL). The combined organic layer was washed with brine, dried over anhydrous Na₂SO₄, filtered, and then evaporated to dryness under

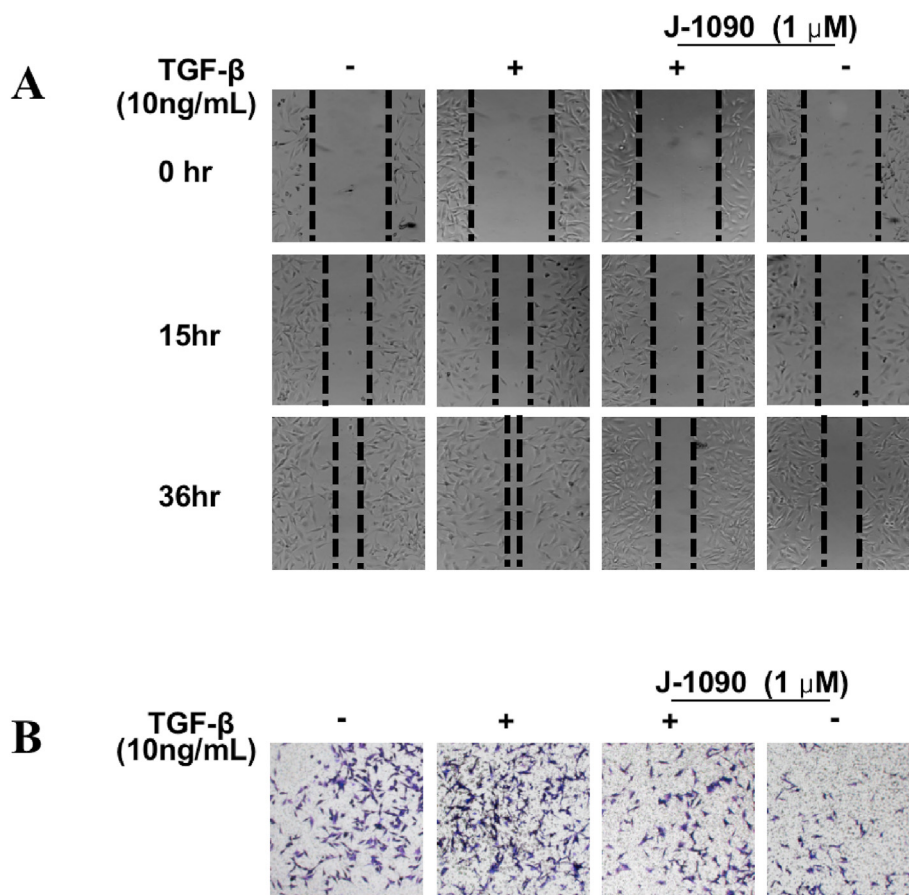


Fig. 8. 13c (J-1090) decreases migration and invasion induced by TGF- β . (A) Representative images of wound healing assay from U87MG cells in control, TGF- β (10 ng/mL), 13c (1 mm), and combination treatment (13c 1 mm + TGF- β 10 ng/mL) for indicated hours. (B) Representative images of matrigel invasion assays from U87MG cells in control, TGF- β (10 ng/mL), 13c (1 mm), and combination treatment (13c 1 mm + TGF- β 10 ng/mL) fixed and stained with 0.1% crystal violet.

reduced pressure. The residue was purified by column chromatography on silica gel using Petroleum ether and ethyl acetate (2:1) as eluent to give the titled compound 16 as a solid.

Yellow solid; Yield 23%; ^1H NMR (300 MHz, CDCl_3) (keto form, 71%) δ 8.57 (s, 1H), 8.13 (d, 2H, $J = 9.0$ Hz), 7.53 (t, 1H, $J = 7.5$ Hz), 7.41 (d, 1H, $J = 9.0$ Hz), 7.12 (d, 1H, $J = 6.0$ Hz), 7.03 (d, 1H, $J = 6.0$ Hz), 4.53 (s, 2H), 4.09 (s, 3H), 2.55 (s, 3H); ^1H NMR (300 MHz, CDCl_3) (enol form, 29%) δ 8.27 (s, 1H), 8.03 (s, 1H), 7.90 (d, 1H, $J = 9.0$ Hz), 7.0 (t, 1H, $J = 7.5$ Hz), 7.41 (d, 1H, $J = 9.0$ Hz), 6.88 (d, 1H, $J = 9.0$ Hz), 6.76 (d, 1H, $J = 6.0$ Hz), 6.08 (s, 1H), 4.06 (s, 3H), 2.54 (s, 3H).

4.1.5. General procedure for the preparation of 1-(1H-indazol-5-yl)-2-(6-methylpyridin-2-yl)ethane-1,2-dione (10) and 1-(1-methyl-1H-indazol-5-yl)-2-(6-methylpyridin-2-yl)ethane-1,2-dione (17)

To a solution of compound 9 or 16 (19.90 mmol) in DMSO (60 mL) at room temperature, 40% HBr in water (17 mL, 79.60 mmol) was added dropwise. The mixture was heated to 70 °C and stirred for 1.5 h. The reaction mixture was cooled to 0 °C in an ice bath, and to it, ice-cold water was added. The pH of the solution was adjusted to 7–8 by adding saturated NaHCO_3 solution. The mixture was extracted with methylene dichloride (3 x 60 mL) and the organic layer was combined. The organic layer was washed with water and brine, dried over anhydrous MgSO_4 , filtered, and then evaporated to dryness under reduced pressure. The residue was purified by column chromatography on silica gel using Petroleum ether and ethyl acetate (4:1) as eluent to give the titled compounds 10 or 17 as a solid.

4.1.5.1. 1-(1H-Indazol-5-yl)-2-(6-methylpyridin-2-yl)ethane-1,2-dione (10). Pale yellow solid; Yield 44%; ^1H NMR (300 MHz, $\text{DMSO}-d_6$) δ 13.61 (s, 1H), 8.31 (d, 2H, $J = 9.0$ Hz), 8.06–8.01 (m, 2H), 7.91 (d, 1H, $J = 9.0$ Hz), 7.71 (d, 1H, $J = 9.0$ Hz), 7.63 (dd, 1H, $J = 6.0, 3.0$ Hz), 2.39 (s, 3H).

4.1.5.2. 1-(1-Methyl-1H-indazol-5-yl)-2-(6-methylpyridin-2-yl)ethane-1,2-dione (17). White solid; Yield 92%; ^1H NMR (300 MHz, $\text{DMSO}-d_6$) δ 8.21 (s, 1H), 8.03 (d, 2H, $J = 6.0$ Hz), 7.98 (t, 1H, $J = 9.0$ Hz), 7.77 (t, 1H, $J = 9.0$ Hz), 7.47 (d, 1H, $J = 9.0$ Hz), 7.34 (d, 1H, $J = 9.0$ Hz), 4.06 (s, 3H), 2.42 (s, 3H).

4.1.6. General procedure for the preparation of 5-(2-(dimethoxymethyl)-5-(6-methylpyridin-2-yl)-1H-imidazole-4-yl)-1H-indazole (11) and 5-(2-(dimethoxymethyl)-5-(6-methylpyridin-2-yl)-1H-imidazole-4-yl)-1-methyl-1H-indazole (18)

To a solution of compound 11 or 17 (9.05 mmol) in MeOH (48 mL) at room temperature, NH_4OAc (89.48 mmol), 60% 2,2-dimethoxyacetaldehyde in H_2O (2.33 mL, 13.30 mmol) and *tert*-butyl methyl ether (48 mL) were added. The reaction mixture was heated to 50 °C and stirred for 2 h. The mixture was cooled to room temperature, and then the solvent was removed by reduced pressure. The residue was cooled to 0 °C and neutralized with saturated NaHCO_3 solution. The mixture was extracted with ethyl acetate (2 x 30 mL) and the combined extracts were washed with water and brine, dried over anhydrous Na_2SO_4 , filtered, and then evaporated to dryness under reduced pressure. The residue was purified by column chromatography on silica gel using methylene

chloride and methanol as eluent to give the titled compounds 11 or 18 as a solid.

4.1.6.1. 5-(2-(Dimethoxymethyl)-5-(6-methylpyridin-2-yl)-1H-imidazole-4-yl)-1H-indazole (11). Pale yellow solid; Yield 64%; ^1H NMR (300 MHz, DMSO- d_6) δ 13.08 (s, 1H, NH), 12.48 (s, 1H, NH), 8.08 (br s, 2H), 7.60 (br s, 2H), 7.49 (d, 1H, $J = 9.0$ Hz), 7.06 (br s, 1H), 5.49 (s, 1H), 3.38 (s, 6H), 2.30 (s, 3H).

4.1.6.2. 5-(2-(Dimethoxymethyl)-5-(6-methylpyridin-2-yl)-1H-imidazole-4-yl)-1-methyl-1H-indazole (18). Pale yellow solid; Yield 54%; ^1H NMR (300 MHz, CDCl_3) δ 10.86 (br s, 1H, NH), 7.99 (d, 2H, $J = 9.0$ Hz), 7.66 (d, 1H, $J = 9.0$ Hz), 7.41 (d, 1H, $J = 9.0$ Hz), 7.35 (t, 1H, $J = 7.5$ Hz), 7.22 (d, 1H, $J = 9.0$ Hz), 6.95 (d, 1H, $J = 6.0$ Hz), 5.58 (s, 1H), 4.10 (s, 3H), 3.45 (s, 6H), 2.53 (s, 3H).

4.1.7. General procedure for the preparation of 4-(1H-indazol-5-yl)-5-(6-methylpyridin-2-yl)-1H-imidazole-2-carbaldehyde (12) and 4-(1-methyl-1H-indazol-5-yl)-5-(6-methylpyridin-2-yl)-1H-imidazole-2-carbaldehyde (19)

Compound 11 or 18 (5.74 mmol) was dissolved in 1 N HCl (18 mL), and the solution was heated at 70 °C for 4 h. The reaction mixture was allowed to cool to 0 °C, and then it was neutralized with saturated NaHCO_3 solution. The yellow precipitates were collected through a Büchner funnel, and the filtered cake was washed with water (2 x 20 mL). The solid was dried in a vacuum oven to give the titled compounds 12 or 19 as a solid.

4.1.7.1. 4-(1H-Indazol-5-yl)-5-(6-methylpyridin-2-yl)-1H-imidazole-2-carbaldehyde (12). Pale yellow solid; Yield 96%; ^1H NMR (300 MHz, DMSO- d_6) δ 13.17 (s, 1H, NH), 9.73 (s, 1H), 8.13 (s, 2H), 7.70 (t, 1H, $J = 7.5$ Hz), 7.61 (d, 1H, $J = 9.0$ Hz), 7.55 (t, 2H, $J = 9.0$ Hz), 7.18 (d, 1H, $J = 6.0$ Hz), 2.37 (s, 3H).

4.1.7.2. 4-(1-Methyl-1H-indazol-5-yl)-5-(6-methylpyridin-2-yl)-1H-imidazole-2-carbaldehyde (19). Pale yellow solid; Yield 93%; ^1H NMR (300 MHz, $\text{CDCl}_3 + \text{DMSO-}d_6$) δ 9.81 (s, 1H), 8.01 (s, 2H), 7.65 (d, 1H, $J = 9.0$ Hz), 7.48 (d, 1H, $J = 9.0$ Hz), 7.41 (t, 1H, $J = 7.5$ Hz), 7.25 (d, 1H, $J = 6.0$ Hz), 7.07 (d, 1H, $J = 9.0$ Hz), 4.31 (s, 3H), 2.58 (s, 3H).

4.1.8. General procedure for the preparation of 2-substituted-4-(1H-indazol-5-yl)-5-(6-methylpyridin-2-yl)-1H-imidazoles 13a–g or 2-substituted-4-(1-methyl-1H-indazol-5-yl)-5-(6-methylpyridin-2-yl)-1H-imidazoles 20a–g

To a stirred solution of 12 or 19 (0.33 mmol) in tetrahydrofuran (THF, 8 mL), were added appropriate substituted anilines (0.50 mmol) and acetic acid (AcOH, 0.33 mmol), and the reaction mixture was heated at 75 °C for 2 h under nitrogen atmosphere. The reaction mixture was cooled to 0 °C, and methanol (3 mL) was added. To it, NaBH_4 (0.06 g, 1.32 mmol) was added portionwise, and then the reaction mixture was allowed to room temperature and stirred for an additional 3 h. The pH of the reaction mixture was adjusted to 7–8 at 0 °C with 1 N HCl, and then the organic layer was separated. The aqueous layer was extracted with methylene chloride (3 x 20 mL). The combined organic layers was washed with water and brine, dried over anhydrous Na_2SO_4 , filtered, and evaporated to dryness under reduced pressure. The residue was purified by column chromatography on silica gel using methylene chloride and methanol as eluent to give the titled compounds 13a–g and 20a–g as solids.

4.1.8.1. N-((4-(1H-indazol-5-yl)-5-(6-methylpyridin-2-yl)-1H-imidazole-2-yl)methyl)aniline (13a). Yellow solid; Yield 67%; mp 216–218 °C; purity by HPLC: 98.87% (DW: acetonitrile = 70:30); ^1H NMR (300 MHz, $\text{CDCl}_3 + \text{DMSO-}d_6$) δ 7.99 (s, 1H), 7.91 (s, 1H), 7.51 (d,

2H, $J = 6.0$ Hz), 7.30 (t, 1H, $J = 9.0$ Hz), 7.18 (d, 2H, $J = 9.0$ Hz), 7.12 (t, 1H, $J = 7.5$ Hz), 6.91 (d, 1H, $J = 6.0$ Hz), 6.71 (d, 2H, $J = 6.0$ Hz), 4.47 (s, 2H), 2.13 (s, 3H); ^{13}C NMR (125 MHz, $\text{CDCl}_3 + \text{CD}_3\text{OD}$) δ 157.91, 148.99, 147.60, 146.99, 139.76, 138.47, 136.87, 134.32, 129.26 (2C), 128.19, 127.05, 126.84, 123.18, 121.33, 121.01, 118.30, 118.19, 113.26 (2C), 110.24, 41.91, 23.95; HRMS-ESI (m/z): $[\text{M} + \text{H}]^+$ calcd for $\text{C}_{23}\text{H}_{21}\text{N}_6$ 381.18222, found 381.18253.

4.1.8.2. N-((4-(1H-indazol-5-yl)-5-(6-methylpyridin-2-yl)-1H-imidazole-2-yl)methyl)-2-fluoroaniline (13b). White solid; Yield 32%; mp 218–220 °C; purity by HPLC: 99.87% (DW: acetonitrile = 70:30); ^1H NMR (300 MHz, $\text{CDCl}_3 + \text{CD}_3\text{OD}$) δ 8.00 (s, 1H), 7.92 (s, 1H), 7.54 (d, 1H, $J = 9.0$ Hz), 7.48 (d, 1H, $J = 9.0$ Hz), 7.31 (t, 1H, $J = 7.5$ Hz), 7.12 (d, 1H, $J = 6.0$ Hz), 6.99–6.90 (m, 3H), 6.77 (t, 1H, $J = 9.0$ Hz), 6.68–6.61 (m, 1H), 4.52 (s, 2H), 2.48 (s, 3H); ^{13}C NMR (125 MHz, $\text{CDCl}_3 + \text{CD}_3\text{OD}$) δ 158.00, 151.82 (d, $J = 237.50$ Hz), 150.87, 149.55, 146.72, 139.83, 136.97, 136.04 (d, $J = 11.25$ Hz), 134.36, 128.32, 127.07, 124.78, 124.76, 123.25, 121.42, 121.06, 118.40, 117.86 (d, $J = 6.25$ Hz), 114.59 (d, $J = 17.5$ Hz), 112.76 (d, $J = 2.5$ Hz), 110.32, 41.63, 24.02; ^{19}F NMR (470 MHz, $\text{CDCl}_3 + \text{CD}_3\text{OD}$) –135.70; HRMS-ESI (m/z): $[\text{M} + \text{H}]^+$ calcd for $\text{C}_{23}\text{H}_{20}\text{FN}_6$ 399.17280, found 399.17273.

4.1.8.3. N-((4-(1H-indazol-5-yl)-5-(6-methylpyridin-2-yl)-1H-imidazole-2-yl)methyl)-3-fluoroaniline (13c). White solid; Yield 40%; mp 229–230 °C; purity by HPLC: 99.65% (DW: acetonitrile = 70:30); ^1H NMR (300 MHz, $\text{CDCl}_3 + \text{CD}_3\text{OD}$) δ 7.92 (s, 1H), 7.82 (s, 1H), 7.44 (s, 2H), 7.03 (t, 2H, $J = 7.5$ Hz), 6.88 (d, 1H, $J = 6.0$ Hz), 6.43–6.31 (m, 4H), 4.37 (s, 2H), 3.53 (s, 3H); ^{13}C NMR (125 MHz, $\text{CDCl}_3 + \text{CD}_3\text{OD}$) δ 164.02 (d, $J = 241.25$ Hz), 157.91, 149.52 (d, $J = 11.25$ Hz), 149.09, 146.47, 139.75, 138.77, 136.91, 134.32, 130.38, 130.30, 128.21, 127.01, 123.20, 121.35, 121.00, 118.29, 110.24, 108.95, 104.49 (d, $J = 21.25$ Hz), 99.94 (d, $J = 25.00$ Hz), 41.69, 23.96; ^{19}F NMR (470 MHz, CD_3OD) –115.31; HRMS-ESI (m/z): $[\text{M} + \text{H}]^+$ calcd for $\text{C}_{23}\text{H}_{20}\text{FN}_6$ 399.17280, found 399.17264.

4.1.8.4. N-((4-(1H-indazol-5-yl)-5-(6-methylpyridin-2-yl)-1H-imidazole-2-yl)methyl)-4-fluoroaniline (13d). White solid; Yield 38%; mp 217–218 °C; purity by HPLC: 99.75% (DW: acetonitrile = 70:30); ^1H NMR (300 MHz, $\text{CDCl}_3 + \text{CD}_3\text{OD}$) δ 7.92 (s, 1H), 7.82 (s, 1H), 7.44 (s, 2H), 7.27 (t, 1H, $J = 9.0$ Hz), 7.04 (d, 1H, $J = 9.0$ Hz), 6.88 (d, 1H, $J = 6.0$ Hz), 6.79 (t, 2H, $J = 7.5$ Hz), 6.61–6.57 (m, 2H), 4.35 (s, 2H), 2.43 (s, 3H); ^{13}C NMR (125 MHz, $\text{CDCl}_3 + \text{CD}_3\text{OD}$) δ 157.92, 156.32 (d, $J = 233.75$ Hz), 153.75, 149.09, 146.81, 143.96, 139.77, 136.90, 134.32, 128.23, 127.10, 123.18, 121.32, 118.22, 115. (d, 2C, $J = 22.5$ Hz), 114.27 (d, 2C, $J = 7.5$ Hz), 110.25, 42.57, 23.98; ^{19}F NMR (470 MHz, $\text{CDCl}_3 + \text{CD}_3\text{OD}$) –127.12; HRMS-ESI (m/z): $[\text{M} + \text{H}]^+$ calcd for $\text{C}_{23}\text{H}_{20}\text{FN}_6$ 399.17280, found 399.17258.

4.1.8.5. N-((4-(1H-indazol-5-yl)-5-(6-methylpyridin-2-yl)-1H-imidazole-2-yl)methyl)-2-methylaniline (13e). Yellow solid; Yield 66%; mp 180–181 °C; purity by HPLC: 96.93% (DW: acetonitrile = 70:30); ^1H NMR (300 MHz, CDCl_3) δ 8.02 (s, 1H), 7.96 (s, 1H), 7.55 (d, 1H, $J = 6.0$ Hz), 7.36–7.28 (m, 2H), 7.20 (d, 1H, $J = 6.0$ Hz), 7.10–7.04 (m, 2H), 6.91 (d, 1H, $J = 6.0$ Hz), 6.72–6.66 (m, 2H), 4.55 (s, 2H), 2.46 (s, 3H), 2.13 (s, 3H); ^{13}C NMR (125 MHz, $\text{CDCl}_3 + \text{CD}_3\text{OD}$) δ 158.01, 149.21, 147.14, 145.66, 139.85, 138.96, 136.96, 134.46, 130.31, 128.34, 127.28, 127.21, 123.33, 122.97, 121.39, 121.11, 118.33, 118.14, 110.39, 110.32, 42.15, 24.10, 17.45; HRMS-ESI (m/z): $[\text{M} + \text{H}]^+$ calcd for $\text{C}_{23}\text{H}_{23}\text{N}_6$ 395.19787, found 395.19778.

4.1.8.6. N-((4-(1H-indazol-5-yl)-5-(6-methylpyridin-2-yl)-1H-imidazole-2-yl)methyl)-3-methylaniline (13f). Pale yellow solid; Yield 56%; mp 188–190 °C; purity by HPLC: 98.66% (DW:

acetonitrile = 70:30); ^1H NMR (300 MHz, CDCl_3) δ 8.01 (s, 1H), 7.93 (s, 1H), 7.56 (d, 1H, $J = 9.0$ Hz), 7.49 (d, 1H, $J = 9.0$ Hz), 7.31 (t, 1H, $J = 7.5$ Hz), 7.13 (d, 1H, $J = 9.0$ Hz), 7.06 (t, 1H, $J = 7.5$ Hz), 6.92 (d, 1H, $J = 9.0$ Hz), 6.55 (t, 3H, $J = 9.0$ Hz), 4.48 (s, 2H), 2.50 (s, 3H), 2.25 (s, 3H); ^{13}C NMR (125 MHz, $\text{CDCl}_3 + \text{CD}_3\text{OD}$) δ 157.94, 149.01, 147.66, 146.99, 139.75, 139.18, 136.84, 134.59, 134.47, 129.21, 128.30, 123.26, 121.24, 121.05, 119.39, 118.01, 114.16, 110.41, 110.19, 42.18, 24.08, 21.51; HRMS-ESI (m/z): $[\text{M} + \text{H}]^+$ calcd for $\text{C}_{23}\text{H}_{23}\text{N}_6$ 395.19787, found 395.19806.

4.1.8.7. *N*-((4-(1H-indazol-5-yl)-5-(6-methylpyridin-2-yl)-1H-imidazole-2-yl)methyl)-4-methylaniline (13 g). Pale yellow solid; Yield 60%; mp 184–185 °C; purity by HPLC: 99.73% (DW: acetonitrile = 70:30); ^1H NMR (300 MHz, CDCl_3) δ 8.04 (s, 1H), 7.96 (s, 1H), 7.58 (dd, 1H, $J = 9.0, 3.0$ Hz), 7.50 (d, 1H, $J = 9.0$ Hz), 7.33 (t, 1H, $J = 7.5$ Hz), 7.16 (d, 1H, $J = 9.0$ Hz), 7.02 (d, 2H, $J = 9.0$ Hz), 6.94 (d, 1H, $J = 9.0$ Hz), 6.68 (d, 2H, $J = 9.0$ Hz), 4.49 (s, 2H), 2.52 (s, 3H), 2.23 (s, 3H); ^{13}C NMR (125 MHz, $\text{CDCl}_3 + \text{CD}_3\text{OD}$) δ 158.03, 149.06, 147.15, 145.38, 139.82, 136.92, 134.59, 129.92 (2C), 128.39, 127.87, 127.31, 123.36, 121.33, 121.16, 118.07, 113.64 (2C), 110.27, 42.61, 24.18, 14.13; HRMS-ESI (m/z): $[\text{M} + \text{H}]^+$ calcd for $\text{C}_{23}\text{H}_{23}\text{N}_6$ 395.19787, found 395.19769.

4.1.8.8. *N*-((4-(1-methyl-1H-indazol-5-yl)-5-(6-methylpyridin-2-yl)-1H-imidazole-2-yl)methyl)aniline (20a). Pale yellow solid; Yield 60%; mp 152–153 °C; purity by HPLC: 99.90% (DW: acetonitrile = 70:30); ^1H NMR (300 MHz, CDCl_3) δ 7.97 (s, 2H), 7.65 (d, 1H, $J = 9.0$ Hz), 7.42 (d, 1H, $J = 9.0$ Hz), 7.33 (t, 1H, $J = 7.5$ Hz), 7.19 (t, 3H, $J = 7.5$ Hz), 6.92 (d, 1H, $J = 9.0$ Hz), 6.77 (t, 1H, $J = 7.5$ Hz), 6.70 (d, 2H, $J = 9.0$ Hz), 4.50 (s, 2H), 4.10 (s, 3H), 2.48 (s, 3H); ^{13}C NMR (125 MHz, CDCl_3) δ 158.12, 148.89, 147.65, 146.43, 139.58, 136.62, 133.15, 129.41 (2C), 127.90, 127.50, 124.34, 121.30, 121.01, 118.57, 117.30, 113.38 (2C), 109.01, 42.80, 35.65, 24.35; HRMS-ESI (m/z): $[\text{M} + \text{H}]^+$ calcd for $\text{C}_{24}\text{H}_{23}\text{N}_6$ 395.19787, found 395.19794.

4.1.8.9. 2-Fluoro-*N*-((4-(1-Methyl-1H-Indazol-5-yl)-5-(6-methylpyridin-2-yl)-1H-imidazole-2-yl)methyl)aniline (20b). Pale yellow solid; Yield 35%; mp 148–150 °C; purity by HPLC: 99.78% (DW: acetonitrile = 70:30); ^1H NMR (300 MHz, CDCl_3) δ 7.99 (s, 1H), 7.97 (s, 1H), 7.67 (d, 1H, $J = 9.0$ Hz), 7.41 (d, 1H, $J = 6.0$ Hz), 7.34 (t, 1H, $J = 7.5$ Hz), 7.21 (d, 1H, $J = 9.0$ Hz), 6.99–6.88 (m, 3H), 6.75 (t, 1H, $J = 7.5$ Hz), 6.71–6.64 (m, 1H), 4.59 (br s, 1H, NH), 4.51 (s, 2H), 4.10 (s, 3H), 2.40 (s, 3H); ^{13}C NMR (125 MHz, CDCl_3) δ 158.12, 151.72 (d, $J = 238.75$ Hz), 148.94, 146.13, 139.57, 136.64, 136.05 (d, $J = 12.5$ Hz), 133.15, 127.85, 127.46, 124.80, 124.77, 124.34, 121.24, 121.05, 117.99, 117.94, 117.50, 114.58 (d, $J = 18.75$ Hz), 112.80, 109.00, 42.43, 35.64, 24.15; ^{19}F NMR (470 MHz, $\text{CDCl}_3 + \text{CD}_3\text{OD}$) –135.58; HRMS-ESI (m/z): $[\text{M} + \text{H}]^+$ calcd for $\text{C}_{24}\text{H}_{22}\text{FN}_6$ 413.18845, found 413.18887.

4.1.8.10. 3-Fluoro-*N*-((4-(1-Methyl-1H-Indazol-5-yl)-5-(6-methylpyridin-2-yl)-1H-imidazole-2-yl)methyl)aniline (20c). Pale yellow solid; Yield 40%; mp 145–146 °C; purity by HPLC: 99.24% (DW: acetonitrile = 70:30); ^1H NMR (300 MHz, CDCl_3) δ 7.96 (s, 2H), 7.65 (d, 1H, $J = 6.0$ Hz), 7.40 (d, 1H, $J = 9.0$ Hz), 7.35 (t, 1H, $J = 9.0$ Hz), 7.21 (d, 1H, $J = 9.0$ Hz), 7.06 (dd, 1H, $J = 15.0, 6.0$ Hz), 6.92 (d, 1H, $J = 6.0$ Hz), 6.43–6.34 (m, 2H), 6.30–6.25 (m, 1H), 4.60 (br s, 1H, NH), 4.37 (s, 2H), 4.09 (s, 3H), 2.43 (s, 3H); ^{13}C NMR (125 MHz, CDCl_3) δ 163.99 (d, $J = 241.25$ Hz), 158.11, 149.34 (d, $J = 10.0$ Hz), 149.02, 145.86, 139.57, 136.77, 135.22, 133.14, 130.46, 130.38, 127.81, 127.24, 125.06, 124.32, 121.21 (d, $J = 12.5$ Hz), 117.60, 109.07, 108.96, 104.77 (d, $J = 21.25$ Hz), 100.05 (d, $J = 25.0$ Hz), 42.32, 35.63, 24.18; ^{19}F NMR (470 MHz, $\text{CDCl}_3 + \text{CD}_3\text{OD}$) –112.37; HRMS-ESI (m/z): $[\text{M} + \text{H}]^+$ calcd for $\text{C}_{24}\text{H}_{22}\text{FN}_6$ 413.18845, found 413.18863.

4.1.8.11. 4-Fluoro-*N*-((4-(1-Methyl-1H-Indazol-5-yl)-5-(6-methylpyridin-2-yl)-1H-imidazole-2-yl)methyl)aniline (20d). Pale yellow solid; Yield 38%; mp 147–148 °C; purity by HPLC: 99.48% (DW: acetonitrile = 70:30); ^1H NMR (300 MHz, CDCl_3) δ 7.98 (s, 2H), 7.65 (d, 1H, $J = 9.0$ Hz), 7.41 (d, 1H, $J = 6.0$ Hz), 7.37 (t, 1H, $J = 9.0$ Hz), 7.22 (d, 1H, $J = 6.0$ Hz), 6.94 (d, 1H, $J = 6.0$ Hz), 6.85 (t, 2H, $J = 9.0$ Hz), 6.58–6.54 (m, 2H), 4.40 (s, 2H), 4.11 (s, 3H), 2.45 (s, 3H); ^{13}C NMR (125 MHz, CDCl_3) δ 158.12, 156.39 (d, $J = 235.00$ Hz), 148.97, 146.28, 143.91, 139.57, 136.70, 135.23, 133.13, 127.83, 127.34, 125.05, 124.33, 121.26, 121.09, 117.44, 115.80 (d, 2C, $J = 21.25$ Hz), 114.24 (d, 2C, $J = 6.25$ Hz), 109.04, 43.24, 35.64, 24.27; ^{19}F NMR (470 MHz, $\text{CDCl}_3 + \text{CD}_3\text{OD}$) –126.70; HRMS-ESI (m/z): $[\text{M} + \text{H}]^+$ calcd for $\text{C}_{24}\text{H}_{22}\text{FN}_6$ 413.18845, found 413.18872.

4.1.8.12. 2-Methyl-*N*-((4-(1-Methyl-1H-Indazol-5-yl)-5-(6-methylpyridin-2-yl)-1H-imidazole-2-yl)methyl)aniline (20e). Pale yellow solid; Yield 61%; mp 150–152 °C; purity by HPLC: 97.27% (DW: acetonitrile = 70:30); ^1H NMR (300 MHz, $\text{CDCl}_3 + \text{CD}_3\text{OD}$) δ 7.98 (s, 2H), 7.65 (d, 1H, $J = 9.0$ Hz), 7.40 (d, 1H, $J = 6.0$ Hz), 7.33 (t, 1H, $J = 7.5$ Hz), 7.20 (d, 1H, $J = 9.0$ Hz), 7.12 (d, 1H, $J = 9.0$ Hz), 7.07 (d, 1H, $J = 6.0$ Hz), 6.91 (d, 1H, $J = 6.0$ Hz), 6.72 (d, 1H, $J = 6.0$ Hz), 6.68 (d, 1H, $J = 6.0$ Hz), 4.53 (s, 2H), 4.10 (s, 3H), 2.46 (s, 3H), 2.18 (s, 3H); ^{13}C NMR (125 MHz, CDCl_3) δ 158.11, 148.99, 146.56, 145.69, 139.57, 136.61, 133.15, 132.48, 130.90, 130.27, 128.82, 127.90, 127.35, 124.33, 122.74, 121.27, 121.01, 118.22, 117.41, 110.52, 108.98, 42.80, 35.64, 24.32, 17.53; HRMS-ESI (m/z): $[\text{M} + \text{H}]^+$ calcd for $\text{C}_{25}\text{H}_{25}\text{N}_6$ 409.21352, found 409.21329.

4.1.8.13. 3-Methyl-*N*-((4-(1-Methyl-1H-Indazol-5-yl)-5-(6-methylpyridin-2-yl)-1H-imidazole-2-yl)methyl)aniline (20f). Pale yellow solid; Yield 58%; mp 150–151 °C; purity by HPLC: 97.92% (DW: acetonitrile = 70:30); ^1H NMR (300 MHz, CDCl_3) δ 7.96 (s, 2H), 7.65 (d, 1H, $J = 9.0$ Hz), 7.40 (d, 1H, $J = 9.0$ Hz), 7.33 (t, 1H, $J = 7.5$ Hz), 7.20 (d, 1H, $J = 9.0$ Hz), 7.05 (t, 1H, $J = 9.0$ Hz), 6.91 (d, 1H, $J = 9.0$ Hz), 6.58 (d, 1H, $J = 9.0$ Hz), 6.46 (d, 2H, $J = 6.0$ Hz), 4.45 (s, 2H), 4.09 (s, 3H), 2.45 (s, 3H), 2.24 (s, 3H); ^{13}C NMR (125 MHz, CDCl_3) δ 158.10, 148.99, 147.71, 146.68, 139.56, 139.18, 136.62, 133.14, 129.26, 127.90, 127.53, 124.33, 124.09, 121.26, 120.99, 119.44, 117.44, 114.19, 110.39, 109.00, 42.73, 35.63, 24.27, 21.61; HRMS-ESI (m/z): $[\text{M} + \text{H}]^+$ calcd for $\text{C}_{25}\text{H}_{25}\text{N}_6$ 409.21352, found 409.21371.

4.1.8.14. 4-Methyl-*N*-((4-(1-Methyl-1H-Indazol-5-yl)-5-(6-methylpyridin-2-yl)-1H-imidazole-2-yl)methyl)aniline (20 g). Pale yellow solid; Yield 60%; mp 155–156 °C; purity by HPLC: 99.54% (DW: acetonitrile = 70:30); ^1H NMR (300 MHz, CDCl_3) δ 7.96 (s, 2H), 7.64 (d, 1H, $J = 9.0$ Hz), 7.39 (d, 1H, $J = 9.0$ Hz), 7.33 (t, 1H, $J = 7.5$ Hz), 7.19 (d, 1H, $J = 9.0$ Hz), 6.98 (d, 2H, $J = 9.0$ Hz), 6.91 (d, 1H, $J = 9.0$ Hz), 6.57 (d, 2H, $J = 9.0$ Hz), 4.42 (s, 2H), 4.09 (s, 3H), 2.45 (s, 3H), 2.22 (s, 3H); ^{13}C NMR (125 MHz, CDCl_3) δ 158.08, 149.14, 146.83, 145.36, 139.55, 136.63, 133.23, 133.13, 130.04, 129.84 (2C), 127.91, 127.71, 127.35, 124.30, 121.27, 121.00, 117.51, 113.51 (2C), 108.99, 42.98, 35.62, 24.25, 20.41; HRMS-ESI (m/z): $[\text{M} + \text{H}]^+$ calcd for $\text{C}_{25}\text{H}_{25}\text{N}_6$ 409.21352, found 409.21332.

4.2. Biology

4.2.1. Kinase assay [21]

All kinase experiments were completed by the ProQinase (Germany). All protein kinases were expressed in Sf9 insect cells or in *E. coli* as recombinant GST-fusion proteins or His-tagged proteins, either as full-length or enzymatically active fragments. A radio-metric protein kinase assay (^{33}P PanQinase® activity assay) was used for measuring the kinase activity of the two protein kinases. All kinase assays were performed in 96-well FlashPlates™ from PerkinElmer (Boston, MA, USA) in 50 mL reaction volumes. The

reaction cocktail was pipetted in four steps in the following order: 20 mL of assay buffer (standard buffer), 5 mL of ATP solution (in H₂O), 5 mL of test compound (in 10% DMSO), 20 mL enzyme/substrate mix. The assay for all protein kinases contained 70 mM HEPES-NaOH pH 7.5, 3 mM MgCl₂, 3 mM MnCl₂, 3 mM Na⁺-orthovanadate, 1.2 mM DTT, 50 mg/mL PEG20000, ATP, [γ -³³P]-ATP, protein kinase, and substrate. The reaction cocktail was incubated at 30 °C for 60 min. The reaction was halted with 50 mL of 2% (v/v) H₃PO₄, plates were aspirated and washed two times with 200 mL 0.9% (w/v) NaCl. Incorporation of ³³Pi was established with a microplate scintillation counter (Microbeta, Wallac). All assays were performed with a BeckmanCoulter/SAGIAN™ Core System.

4.2.2. Docking study

All molecular computation studies were carried out using Discovery Studio 2017.

(Accelrys, San Diego, USA). The X-ray crystal structures of ALK5 complexed with

5,6-dihydro-4H-pyrrolo[1,2-b]pyrazole inhibitor and p38 α complexed with SB203580 were obtained from protein data bank, respectively. (PDB ID: 1RW8 and 1A9U). The water molecules in protein were removed and the protein was prepared by adding hydrogen and correcting incomplete residues using Clean Protein tool of DS, then the protein was refined with CHARMM. The structures of ligands (13c and 20 g) were sketched in 2D and converted into 3D using the DS molecule editor. Automated docking studies were carried out to investigate the binding mode of ligands in the crystal structure utilizing Libdock protocol.

4.2.3. Cell culture and reagents

U87MG cells were purchased from American Type Culture Collection (Manassas, VA, USA). The cells were maintained at 37 °C under 5% CO₂ in DMEM supplemented with 10% heat-inactivated fetal bovine serum (FBS, Hyclone, Logan, UT, USA) and penicillin (100 units/mL)-streptomycin (100 μ g/mL) (Invitrogen, Carlsbad, CA, USA). Transforming growth factor- β (TGF- β) was bought from R&D Systems. Temozolomide (TMZ) was purchased from Meilunbio (Dalian, CHN).

4.2.4. Immunoblot analysis

U87MG cells were seeded in each of 35-mm dishes. After 12-h incubation, cells were either untreated or treated with 10 ng/mL TGF- β in the presence of 5 or 13c, and then harvested at 48 h. Protein lysates were prepared in ice-cold lysis buffer (50 mM Tris-HCl, pH 7.5, 1% Nonidet P-40, 1 mM EDTA, 150 mM NaCl, 1 mM phenylmethylsulfonyl fluoride) with the protease inhibitor cocktail (BD Biosciences, San Diego, CA, USA) added. Equal amounts of protein lysates were separated by SDS-polyacrylamide gel and transferred to a polyvinylidene difluoride membrane (Millipore, Bedford, MA, USA). The membrane was blocked with 5% skim milk and subsequently incubated overnight at 4 °C with primary antibodies against Slug (Santa Cruz; Dallas, TX, USA), N-cadherin (Cell Signaling Technology, Beverly, MA, USA), Vimentin (Cell Signaling Technology) and α -tubulin (Sigma-Aldrich; St. Louis, MO, USA). After binding of an indicated secondary antibody conjugated with horseradish peroxidase, proteins were visualized by enhanced chemiluminescence (Amersham Pharmacia Biotec, Buckinghamshire, UK).

4.2.5. Immunofluorescence assay

U87MG cells (1 \times 10⁴ cells/well) were seeded into 24-well plates. Cells were incubated to adhere at 37 °C overnight and treated with or without TGF- β (10 ng/mL) in the presence or absence of 13c (1 μ M) for 48 h. Cells untreated or treated with TGF- β were used as negative and positive controls respectively.

Afterward, cells were rinsed in PBS and fixed in fresh 4% paraformaldehyde at room temperature for 30 min, followed by 0.2% Triton X-100 for permeabilization. Cells were blocked with 5% BSA in PBS for 30 min and incubated overnight with the primary antibodies at 4 °C. After washed three times in PBS, cells were further incubated with the secondary antibodies for 30 min at room temperature and then counterstained with DAPI for 30 min to label nuclei. Images were acquired by confocal laser-scanning microscope (Nikon, Japan) and merged using NIS-Elements software (Nikon) to produce cyan fluorescence in areas of co-localization.

4.2.6. Cell migration and invasion assays

Cell migration was determined by using a wound healing assay. U87MG cells were reseeded onto 24-well plate (1 \times 10⁵ cells/well), each well was incubated with 1 mL DMEM medium containing 10% FBS. When cells reached approximately 80% confluence, the monolayer cells were scratched with a pipette tip in a straight line and subsequently washed with PBS. Wounded cells were immediately placed in 0.1% FBS-containing medium supplemented with TGF- β (10 ng/mL) in the presence or absence of 13c (1 μ M). Images of wells were obtained at 0, 15, and 36 h under a bright field microscope.

The invasion behavior of cells was measured using the Transwell Matrigel assay (Corning, USA, pore size 8 μ m). Cells were seeded into 6-well plates. After treated with or without TGF- β (10 ng/mL) in the presence or absence of 13c (1 μ M), cells were trypsinized, counted, and plated (2 \times 10⁴ cells/well) into the upper chambers in serum-free medium. Media containing 20% FBS was added to the lower chamber as a chemoattractant. After incubation for 24 h, non-migrating cells were removed with a cotton swab. Invaded cells were fixed with 4% paraformaldehyde after 24 h and stained with 0.1% crystal violet. Images were captured with a light microscope at \times 200 magnification.

4.2.7. RT-PCR analysis

Total RNA from U87MG cells were obtained using RNA Mini kit (Qiagen, Valencia, CA, USA). Reverse transcription-PCR was performed with RT-PCR kit (Invitrogen) according to the manufacturer's instructions. The primers are as follows: 5'-TGCGGTA-CAGTGTAACTGGG-3' (sense) and 5'-GAAACCGGGCTATCTGCTC G-3' (antisense) for N-cadherin; 5'-GAAGAGAACCTTGCCGTTGAAG-3' (sense) and 5'-GAGAAATCTGCTCTCCTCG-3' (antisense) for Vimentin; 5'-ACCACAG TCCATGCCATCAC-3' (sense) and 5'-TCCAC-CACCCTGTTGCTGTA-3' (antisense) for GAPDH.

4.2.8. Statistical analysis

All experiments were independently performed three times. Data are presented as means \pm S.D. of three experiments. Analysis was performed using a Student's t-test or One-way analysis of variance (ANOVA). A *P* value of less than 0.05 was considered statistically significant in all cases.

Declaration of competing interest

The authors declare that they have no known competing financial interests or personal relationships that could have appeared to influence the work reported in this paper.

Acknowledgments

This work was supported by the National Natural Science Foundation of China (No. 81560557, 81660608 and 81760657). We thank Joe Barber Jr., PhD, from Liwen Bianji, Edanz Editing China (www.liwenbianji.cn/ac), for editing the English text of a draft of this manuscript.

Appendix A. Supplementary data

Supplementary data to this article can be found online at <https://doi.org/10.1016/j.ejmech.2021.113311>.

References

- [1] A. Omuro, L.M. DeAngelis, Glioblastoma and other malignant gliomas: a clinical review, *J. Am. Med. Assoc.* 310 (2013) 1842–1850.
- [2] Q.T. Ostrom, G. Cioffi, H. Gittleman, N. Patil, K. Waite, C. Kruchko, J.S. Barnholtz-Sloan, CBRUS statistical report: primary brain and other central nervous system tumors diagnosed in the United States in 2012–2016, *Neuro. Oncol.* 21 (2019) v1–v100.
- [3] M.M. Georgescu, A. Olar, Genetic and histologic spatiotemporal evolution of recurrent, multifocal, multicentric and metastatic glioblastoma, *Acta. Neuro-pathol. Commun.* 8 (2020) 10.
- [4] J. Tang, B. Yu, Y. Li, W. Zhang, A.A. Alvarez, B. Hu, TGF- β -activated lncRNA LINC00115 is a critical regulator of glioma stem-like cell tumorigenicity, *EMBO Rep.* 20 (2019), e48170.
- [5] J. Seoane, TGF beta and cancer initiating cells, *Cell Cycle* 8 (2009) 3787–3788.
- [6] A. Bruna, R.S. Darken, F. Rojo, A. Ocaña, S. Peñuelas, A. Arias, R. Paris, A. Tortosa, J. Mora, J. Baselga, J. Seoane, High TGF beta-Smad activity confers poor prognosis in glioma patients and promotes cell proliferation depending on the methylation of the PDGF-B gene, *Canc. Cell* 11 (2007) 147–160.
- [7] L.M. Wakefield, A.B. Roberts, TGF- β signaling: positive and negative effects on tumorigenesis, *Curr. Opin. Genet. Dev.* 12 (2002) 22–29.
- [8] C. Wang, M. Zheng, Y. Choi, J. Jiang, L. Li, J. Li, C. Xu, Z. Xian, Y. Li, H. Piao, L. Li, G. Yan, Cryptotanshinone attenuates airway remodeling by inhibiting cross-talk between tumor necrosis factor-like weak inducer of apoptosis and transforming growth factor beta 1 signaling pathways in asthma, *Front. Pharmacol.* 10 (2019) 1338.
- [9] G. Cantelli, E. Crosas-Molist, M. Georgouli, V. Sanz-Moreno, TGF- β -induced transcription in cancer, *Semin. Canc. Biol.* 42 (2017) 60–69.
- [10] G.J. Fournier Pierrick, P. Juárez, G. Jiang, G.A. Clines, M. Niewolna, H.S. Kim, H.W. Walton, X.H. Peng, Y. Liu, K.S. Mohammad, C.D. Wells, J.M. Chirgwin, T.A. Guise, The TGF- β signaling regulator PMEPA1 suppresses prostate cancer metastases to bone, *Canc. Cell* 27 (2015) 809–821.
- [11] J. Massagué, TGF- β signaling in context, *Nat. Rev. Mol. Cell Biol.* 13 (2012) 616–630.
- [12] M. Pickup, S. Novitskiy, H.L. Moses, The roles of TGF- β in the tumour progression and response to therapy, *Cancer Lett.* 356 (2015) 321–331.
- [13] Z. Guo, X. Song, L.M. Zhao, M.G. Piao, J. Quan, H.R. Piao, C.H. Jin, Synthesis and biological evaluation of novel benzo[c][1,2,5]thiadiazol-5-yl and thieno[3,2-c]pyridin-2-yl imidazole derivatives as ALK5 inhibitors, *Bioorg. Med. Chem. Lett.* 29 (2019) 2070–2075.
- [14] S.D. Byfield, C. Major, N.J. Laping, A.B. Roberts, SB-505124 is a selective inhibitor of transforming growth factor-beta type I receptors ALK4, ALK5, and ALK7, *Mol. Pharmacol.* 65 (2004) 744–752.
- [15] C.H. Jin, M. Krishnaiah, D. Sreenu, V.B. Subrahmanyam, K.S. Rao, H.J. Lee, S.J. Park, H.J. Park, K. Lee, Y.Y. Sheen, D.K. Kim, Discovery of N-((4-((1,2,4)triazolo[1,5-a]pyridin-6-yl)-5-(6-methylpyridin-2-yl)-1H-imidazole-2-yl)methyl)-2-fluoroaniline (EW-7197): a highly potent, selective, and orally bioavailable inhibitor of TGF- β type I receptor kinase as cancer immunotherapeutic/antifibrotic agent, *J. Med. Chem.* 57 (2014) 4213–4238.
- [16] F. Gellibert, J. Woolven, M.H. Fouchet, N. Mathews, H. Goodland, V. Lovegrove, A. Laroze, V.L. Nguyen, S. Sauter, R. Wang, C. Janson, W. Smith, G. Krysa, V. Boullay, A.C. de Gouvillat, S. Huet, D. Hartely, Identification of 1,5-naphthyridine derivatives as a novel series of potent and selective TGF- β type I receptor inhibitors, *J. Med. Chem.* 47 (2004) 4494–4506.
- [17] S.D. Barrett, M.L. Boys, H. Chen, J.B. Kramer, Therapeutic Pyrazolyl Thieno Pyridines, 2008. US 20080090861 A1.
- [18] L. Bueno, D.P. de Alwis, C. Pitou, J. Yingling, M. Lahn, S. Glatt, I. Troconiz, Semimechanistic modeling of the tumour growth inhibitory effects of LY2157299, a new type I receptor TGF-beta kinase antagonist, in mice, *Eur. J. Cancer.* 44 (2008) 142–150.
- [19] Y. Fujiwara, H. Nokihara, Y. Yamada, N. Yamamoto, K. Sunami, H. Utsumi, H. Asou, O. Takahashi, K. Ogasawara, I. Gueorguieva, T. Tamura, Phase I study of galunisertib, a TGF-beta receptor I kinase inhibitor, in Japanese patients with advanced solid tumors, *Cancer. Chemother. Pharmacol.* 76 (2015) 1143–1152.
- [20] A.A. Brandes, A.F. Carpentier, S. Kesari, J.M. Sepulveda-Sanchez, H.R. Wheeler, O. Chinot, L. Cher, J.P. Steinbach, D. Capper, P. Specenier, J. Rodon, A. Cleverly, C. Smith, I. Gueorguieva, C. Miles, S.C. Guba, D. Desai, M.M. Lahn, W. Wick, A phase II randomized study of galunisertib monotherapy or galunisertib plus lomustine compared with lomustine monotherapy in patients with recurrent glioblastoma, *Neuro Oncol.* 18 (2016) 1146–1156.
- [21] L. Kwok, J.D. Larson, M. Sabat, Pyrazolo[4,3-b]pyridin-7-amine Inhibitors of ALK5, 2011. WO 2011146287 A1.
- [22] W.J. Zhu, B.W. Cui, H.M. Wang, J.X. Nan, H.R. Piao, L.H. Lian, C.H. Jin, Design, synthesis, and antifibrosis evaluation of 4-(benzo-[c][1,2,5]thiadiazol-5-yl)-3(5)-(6-methyl-pyridin-2-yl)pyrazole and 3(5)-(6-methylpyridin-2-yl)-4-(thieno[3,2-c]pyridin-2-yl)pyrazole derivatives, *Eur. J. Med. Chem.* 180 (2019) 15–27.
- [23] Z.H. Zhang, C. Mi, K.S. Wang, Z. Wang, M.Y. Li, H.X. Zuo, G.H. Xu, X. Li, L.X. Piao, J. Ma, X. Jin, Chelidonine inhibits TNF-induced inflammation by suppressing the NF- κ B pathways in HCT116 cells, *Phytother Res.* 32 (2018) 65–75.
- [24] J. Ma, C. Mi, K.S. Wang, J.J. Lee, X. Jin, 4',6-Dihydroxy-4-methoxyisourone inhibits TNF-alpha-induced NF-kappa B activation and expression of NF-kappa B-regulated target gene products, *J. Pharmacol. Sci.* 130 (2016) 43–50.
- [25] L. Pang, C. Liu, G.H. Gong, Z.S. Q. Synthesis, in vitro and in vivo biological evaluation of novel lappaconitine derivatives as potential anti-inflammatory agents, *Acta Pharm. Sin. B.* 10 (2020) 628–645.
- [26] Y. Xing, C. Mi, Z. Wang, Z.H. Zhang, M.Y. Li, H.X. Zuo, J.Y. Wang, X. Jin, J. Ma, Fraxinellone has anticancer activity in vivo by inhibiting programmed cell death-ligand 1 expression by reducing hypoxia-inducible factor-1 α and Stat3, *Pharmacol. Res.* 135 (2018) 166–180.
- [27] C. Mi, Z. Wang, M.Y. Li, Z.H. Zhang, J. Ma, X. Jin, Zinc finger protein 91 positively regulates the production of il-1 β in macrophages by activation of mapks and non-canonical caspase-8 inflammasome, *Br. J. Pharmacol.* 175 (2018) 4338–4352.
- [28] J. Li, L. Xu, R. Sang, Y. Yu, B. Ge, X. Zhang, Immunomodulatory and anti-inflammatory effects of total flavonoids of Astragalus by regulating nf- κ b and mapk signalling pathways in raw 264.7 macrophages, *Pharmazie* 73 (2018) 589–593.
- [29] R.P. Gangwal, N.R. Das, K. Thanki, M.V. Damre, G.V. Dhoke, S.S. Sharma, S. Jain, A.T. Sangamwar, Identification of p38 α MAP kinase inhibitors by pharmacophore based virtual screening, *J. Mol. Graphics. Modell.* 49 (2014) 18–24.
- [30] K.D. Jerome, M.E. Hepperle, J.K. Walker, L. Xing, R.V. Devraj, A.G. Benson, J.E. Baldus, S.R. Selness, Discovery of 5-substituted-N-arylpiperidazines as inhibitors of p38 MAP kinase, *Bioorg. Med. Chem. Lett.* 20 (2010) 3146–3149.
- [31] Y. Shang, X.F. Li, M.J. Jin, Y. Li, Y.L. Wu, Q. Jin, Y. Zhang, X. Li, M. Jiang, B.W. Cui, L.H. Lian, J.X. Nan, Leucodin attenuates inflammatory response in macrophages and lipid accumulation in steatoic hepatocytes via P2x7 receptor pathway: a potential role in alcoholic liver disease, *Biomed. Pharmacother.* 107 (2018) 374–381.
- [32] A.K. Greenberg, S. Basu, J. Hu, T.A. Yie, K.M. Tchou-Wong, W.N. Rom, T.C. Lee, Selective p38 activation in human non-small cell lung cancer, *Am. J. Respir. Cell Mol. Biol.* 26 (2002) 558–564.
- [33] L. Chen, J.A. Mayer, T.I. Krisko, C.W. Speers, T. Wang, S.G. Hilsenbeck, P.H. Brown, Inhibition of the p38 kinase suppresses the proliferation of human ER-negative breast cancer cells, *Cancer. Res.* 69 (2009) 8853–8861.
- [34] P. Sun, W. Huang, L. Kang, M. Jin, B. Fan, H. Jin, Q.M. Wang, Z. Gao, siRNA-loaded poly (histidine-arginine) (6)-modified chitosan nanoparticle with enhanced cell penetrating and endosomal escape capacities for suppressing breast tumor metastasis, *Int. J. Nanomed.* 12 (2017) 3221–3234.
- [35] K. Gill, B.K. Mohanti, M.S. Ashraf, A.K. Singh, D. Dey, Quantification of p38alpha MAP kinase: a prognostic marker in HNSCC with respect to radiation therapy, *Clin. Chim. Acta* 413 (2012) 219–225.
- [36] I. Baldwin, P. Bamboroough, C.G. Haslam, S.S. Hunjan, T. Longstaff, C.J. Mooney, S. Patel, J. Quinn, D.O. Somers, Kinase array design, back to front: biaryl amides, *Bioorg. Med. Chem. Lett.* 18 (2008) 5285–5289.
- [37] K.M. Amin, Y.M. Syam, M.M. Anwar, H.I. Ali, T.M. Abdel-Ghani, A.M. Serry, Synthesis and molecular docking studies of new furochromone derivatives as p38 α MAPK inhibitors targeting human breast cancer MCF-7 cells, *Bioorg. Med. Chem. Lett.* 25 (2017) 2423–2436.
- [38] F.M. Awadallah, S.M. Abou-Seri, M.M. Abdulla, H.H. Georgey, Design and synthesis of potent 1,2,4-trisubstituted imidazolone derivatives with dual p38 MAPK and ERK1/2 inhibitory activity, *Eur. J. Med. Chem.* 94 (2015) 397–404.
- [39] J. Han, Y. Chen, C. Yang, T. Liu, M. Wang, H. Xu, L. Zhang, C. Zheng, Y. Song, J. Zhu, Structure-based optimization leads to the discovery of NSC765844, a highly potent, less toxic and orally efficacious dual PI3K/mTOR inhibitor, *Eur. J. Med. Chem.* 122 (2016) 684–701.
- [40] Z. Pan, Y. Chen, J. Liu, Q. Jiang, S. Yang, L. Guo, G. He, Design, synthesis, and biological evaluation of polo-like kinase 1/eukaryotic elongation factor 2 kinase (PLK1/EEF2K) dual inhibitors for regulating breast cancer cells apoptosis and autophagy, *Eur. J. Med. Chem.* 144 (2018) 517–528.
- [41] Y.W. Li, X.Y. Li, S. Li, L.M. Zhao, J. Ma, H.R. Piao, Z. Jiang, C.H. Jin, X. Jin, Synthesis and evaluation of the HIF-1 α inhibitory activity of 3(5)-substituted-4-(quinolin-4-yl)- and 4-(2-phenylpyridin-4-yl)pyrazoles as inhibitors of ALK5, *Bioorg. Med. Chem. Lett.* 30 (2019), 126822.
- [42] C.H. Jin, M. Krishnaiah, D. Sreenu, V.B. Subrahmanyam, H.J. Park, S.J. Park, Y.Y. Sheen, D.K. Kim, 4-((1,2,4)triazolo[1,5-a]pyridin-6-yl)-5-(3(5)-(6-methylpyridin-2-yl)imidazole and -pyrazole derivatives as potent and selective inhibitors of transforming growth factor- β type I receptor kinase, *Bioorg. Med. Chem.* 22 (2014) 2724–2732.
- [43] I. Akritopoulou-Zanze, B.D. Wakefield, H. Mack, S.C. Turner, A.F. Gasielki, V.J. Gracias, K.A. Sarris, D.M. Kalvin, M.J. Michmerhuizen, Q. Shuai, J.R. Patel, M.H.M. Bakker, N. Teusch, E.F. Johnson, P.J. Kovar, S.W. Djuric, A.J. Long, A. Vasudevan, D. George, L. Wang, B. Li, N.S. John Moore, A.D. Hobson, K.W. Woods, J.M. Miyashiro, S.L. Swann, T.D. Penning, 5-Substituted Indazoles as Kinase Inhibitors, 2009. US 20090203690 A1.
- [44] M. Journet, D. Cai, R.D. Larsen, P.J. Reider, An improved and practical procedure for the synthesis of substituted phenylacetylpyridines, *Tetrahedron Lett.* 39 (1998) 1717–1720.
- [45] W.C. Lee, C. Chuaqui, L. Sun, M. Hoemann, D. Niu, D. Yan, D. Bonafoux, M. Cornebise, Transforming Growth Factor Modulators, 2007. WO 2007076127 A2.

- [46] M. Krishnaiah, C.H. Jin, D. Sreenu, V.B. Subrahmanyam, K.S. Rao, D.H. Son, H.J. Park, S.W. Kim, Y.Y. Sheen, D.K. Kim, Synthesis and biological evaluation of 2-benzylamino-4(5)-(6-methylpyridin-2-yl)-5(4)-([1,2,4]triazolo[1,5- α]-pyridin-6-yl)thiazoles as transforming growth factor- β type 1 receptor kinase inhibitors, *Eur. J. Med. Chem.* 57 (2012) 74–84.
- [47] T. Mohamed, P.P.N. Rao, 2,4-Disubstituted quinazolines as amyloid- β aggregation inhibitors with dual cholinesterase inhibition and antioxidant properties: development and structure-activity relationship (SAR) studies, *Eur. J. Med. Chem.* 126 (2017) 823–843.
- [48] L.M. Zhao, Z. Guo, Y.J. Xue, J.Z. Min, W.J. Zhu, X.Y. Li, H.R. Piao, C.H. Jin, Synthesis and evaluation of 3-substituted-4-(quinoxalin-6-yl)pyrazoles as TGF- β type I receptor kinase inhibitors, *Molecules* 23 (2018) 3369.
- [49] F. Gellibert, M.H. Fouchet, V.L. Nguyen, R. Wang, G. Krysa, A.C. de Gouville, S. Huet, N. Dodic, Design of novel quinazoline derivatives and related analogues as potent and selective ALK5 inhibitors, *Bioorg. Med. Chem. Lett* 19 (2009) 2277–2281.
- [50] R.D.O. Lopes, N.C. Romeiro, C.K.F. de Lima, L.L.D. Silva, A.L.P.D. Miranda, P.G.B.D. Nascimento, F.Q. Cunha, E.J. Barreiro, L.M. Lima, Docking, synthesis and pharmacological activity of novel urea-derivatives designed as p38 MAPK inhibitors, *Eur. J. Med. Chem.* 54 (2012) 264–271.
- [51] K. Gill, A.K. Singh, V. Kapoor, L. Nigam, R. Kumar, P. Holla, S.N. Das, S. Yadav, N. Subbarao, B.K. Mohanti, S. Dey, Development of peptide inhibitor as therapeutic agent against head and neck squamous cell carcinoma (HNSCC) targeting p38 α MAP kinase, *Biochem. Biophys. Acta.* 1830 (2013) 2763–2769.
- [52] D. Hanahan, R.A. Weinberg, Hallmarks of cancer: the next generation, *Cell* 144 (2011) 646–674.
- [53] M. Diepenbruck, G. Christofori, Epithelial-mesenchymal transition (EMT) and metastasis: yes, no, maybe? *Curr. Opin. Cell Biol.* 43 (2016) 7–13.
- [54] H. Yang, B. David, T.D. Peter, TGF- β -Mediated epithelial-mesenchymal transition and cancer metastasis, *Int. J. Mol. Sci.* 20 (2019) 2767.
- [55] I. Pastushenko, C. Blanpain, EMT transition states during tumor progression and metastasis, *Trends Cell Biol.* 29 (2019) 212–226.
- [56] J.Y. Wang, Z. Wang, M.Y. Li, Z. Zhang, C. Mi, H.X. Zuo, Y. Xing, Y.L. Wu, L.H. Lian, G.H. Xu, L.X. Piao, J. Ma, X. Jin, Dictamnine promotes apoptosis and inhibits epithelial-mesenchymal transition, migration, invasion and proliferation by downregulating the Hif-1 α and Slug signaling pathways, *Chem. Biol. Interact.* 296 (2018) 134–144.
- [57] R. Qureshi, H. Arora, M.A. Rizvi, EMT in cervical cancer: its role in tumour progression and response to therapy, *Cancer Lett.* 356 (2015) 321–331.
- [58] M. Pickup, S. Novitskiy, H.L. Moses, The roles of TGF β in the tumour micro-environment, *Nat. Rev. Cancer.* 13 (2013) 788–799.
- [59] K.M. Hajra, D.Y. Chen, E.R. Fearon, The SLUG zinc-finger protein represses E-cadherin in breast cancer, *Cancer Res.* 62 (2002) 1613–1618.
- [60] V. Maturi, A. Morén, S. Enroth, C.H. Heldin, A. Moustakas, Genomewide binding of transcription factor Snail1 in triple-negative breast cancer cells, *Mol. Oncol.* 12 (2018) 1153–1174.
- [61] D. Wu, B. Zhao, X. Qi, F. Peng, H. Fu, X. Chi, Q. Robert Miao, S. Shao, Nogo-B receptor promotes epithelial-mesenchymal transition in non-small cell lung cancer cells through the Ras/ERK/Snail1 pathway, *Cancer Lett.* 418 (2018) 135–146.
- [62] U.D. Kahlert, G. Nikkhah, J. Maciaczyk, Epithelial-to-mesenchymal(-like) transition as a relevant molecular event in malignant gliomas, *Cancer Lett.* 331 (2013) 131–138.
- [63] J. Seoane, R.R. Gomis, TGF- β family signaling in tumor suppression and cancer progression, *Cold. Spring. Harb. Perspect. Biol.* 9 (2017) a02227.
- [64] S. Ikeno, N. Nakano, K. Sano, T. Minowa, W. Sato, R. Akatsu, N. Sakata, N. Hanagata, M. Fuji, F. Itoh, S. Itoh, PDZK1-interacting protein 1 (PDZK1IP1) traps Smad4 protein and suppresses transforming growth factor- β (TGF- β) signaling, *J. Biol. Chem.* 294 (2019) 4966–4980.